RADIAL POINT INTERPOLATION METHOD FOR PLANE ELASTICITY PROBLEMS

A THESIS SUBMITTED TO
THE GRADUATE SCHOOL OF NATURAL AND APPLIED SCIENCES
OF
MIDDLE EAST TECHNICAL UNIVERSITY

BY

OKAN YILDIRIM

IN PARTIAL FULFILLMENT OF THE REQUIREMENTS
FOR
THE DEGREE OF MASTER OF SCIENCE
IN
MECHANICAL ENGINEERING

SEPTEMBER 2010

Approval of the thesis:

RADIAL POINT INTERPOLATION METHOD FOR PLANE ELASTICITY PROBLEMS

submitted by **OKAN YILDIRIM** in partial fulfillment of the requirements for the degree of **Master of Science in Mechanical Engineering Department, Middle East Technical University** by,

Prof. Dr. Canan Özgen _____
Dean, Graduate School of **Natural and Applied Sciences**

Prof. Dr. Suha Oral _____
Head of Department, **Mechanical Engineering**

Prof. Dr. Suha Oral _____
Supervisor, **Mechanical Engineering Dept., METU**

Examining Committee Members:

Prof. Dr. Ahmet Bülent Doyum _____
Mechanical Engineering Dept., METU

Prof. Dr. Suha Oral _____
Mechanical Engineering Dept., METU

Prof. Dr. Haluk Darendeliler _____
Mechanical Engineering Dept., METU

Asst. Prof. Dr. İlhan Konukseven _____
Mechanical Engineering Dept., METU

Prof. Dr. Mehmet Utku _____
Civil Engineering Dept., METU

Date: 16.09.2010

I hereby declare that all information in this document has been obtained and presented in accordance with academic rules and ethical conduct. I also declare that, as required by these rules and conduct, I have fully cited and referenced all material and results that are not original to this work.

Name, Last name : Okan Yıldırım

Signature :

ABSTRACT

RADIAL POINT INTERPOLATION METHOD
FOR PLANE ELASTICITY PROBLEMS

Yıldırım, Okan

M.Sc., Department of Mechanical Engineering

Supervisor: Prof. Dr. Suha Oral

September 2010, 72 pages

Meshfree methods have become strong alternatives to conventional numerical methods used in solid mechanics after significant progress in recent years. Radial point interpolation method (RPIM) is a meshfree method based on Galerkin formulation and constructs shape functions which enable easy imposition of essential boundary conditions. This thesis analyses plane elasticity problems using RPIM. A computer code implementing RPIM for the solution of plane elasticity problems is developed. Selected problems are solved and the effect of shape parameters on the accuracy of RPIM with and without polynomial terms added in the interpolation is studied. The optimal shape parameters are determined for plane elasticity problems.

Keywords: Meshfree methods, radial basis function, plane elasticity

ÖZ

DÜZLEM ELASTİSİTE PROBLEMLERİ İÇİN RADYAL NOKTA İNTERPOLASYON YÖNTEMİ

Yıldırım, Okan
Yüksek Lisans, Makina Mühendisliği Bölümü
Tez Yöneticisi: Prof. Dr. Suha Oral

Eylül 2010, 72 sayfa

Ağsız yöntemler son yıllardaki önemli gelişmelerin ardından katı mekaniğinde kullanılan klasik sayısal yöntemlere güçlü alternatifler olmuşlardır. Radyal nokta interpolasyon yöntemi (RNİY) Galerkin formulasyonuna dayanan bir ağsız yöntemdir ve sınır koşullarının kolayca uygulanmasını sağlayan şekil fonksiyonları oluşturur. Bu tez RNİY'yi kullanarak düzlem elastisite problemlerini analiz eder. Düzlem elastisite problemlerinin çözümü için RNİY'yi kullanan bir bilgisayar kodu geliştirilmiştir. Seçilen problemler çözülmüş ve şekil parametrelerinin RNİY'nin doğruluğu üzerindeki etkileri interpolasyonda polinom terimleri eklenmiş ve eklenmemiş halde çalışılmıştır. Düzlem elastisite problemleri için en uygun şekil parametreleri belirlenmiştir.

Anahtar Kelimeler: Ağsız yöntemler, radyal tabanlı foksiyon, düzlem elastisite

TABLE OF CONTENTS

LIST OF TABLES

TABLES

LIST OF FIGURES

FIGURES

LIST OF SYMBOLS

σ	Stress
ε	Strain
u, v	Displacements in x and y directions
υ	Poisson's ratio
E	Modulus of elasticity
$\mathbf{D}$	Elasticity matrix
b	Body force
t	Surface traction
B	Basis function
R	Radial basis function
p	Polynomial basis function
ϕ	Shape function
c, q	Shape parameters of MQ radial basis function
$\mathbf{R}_0$	Moment matrix of radial basis functions

$\mathbf{P}_m$ Moment matrix of polynomial terms

$\mathbf{B}$ Strain-displacement matrix

$\mathbf{K}_{ij}$ Nodal stiffness matrix

$\mathbf{K}$ Global Stiffness matrix

$\mathbf{f}_i^b$ Nodal body force vector

$\mathbf{f}_i^t$ Nodal traction force vector

$\mathbf{F}^b$ Global body force vector

$\mathbf{F}^t$ Global traction force vector

$\mathbf{U}$ Global displacement vector

CHAPTER 1

INTRODUCTION

For the simulation of physical problems, partial differential equations which govern the physical phenomena in the problem have to be solved. In most of the cases, it is difficult to obtain an exact solution of the partial differential equation for a real problem due to complexity of the problem. Conventional approach for the solutions of these partial differential equations is to use numerical methods where the solutions are approximated. A number of powerful numerical methods such as the finite difference method (FDM), the finite volume method (FVM) and the finite element method (FEM) have been developed using the idea of transforming a complex problem of partial differential equations into a simple discrete mathematical model. The common feature of these methods is the reliance on a mesh. In all these methods, the problem domain where the partial differential equations are defined are discretized into subdomains. A continuous domain of these discrete subdomains forms a mesh and a priori connectivity information between nodes introduced in the problem domain for the discretization is required.

The finite element method (FEM) is very well established mesh based numerical method for the solution of the partial differential equations in the most of engineering solid mechanics problems. It discretizes the problem domain into meshes, so called elements, with predefined connectivity between nodes. The solution in each element is approximated by shape functions. Then applying proper formulation principles and using element based shape functions, a set of discrete system of equations for the discretized problem domain is formed. Although the

FEM is the most frequently used and dominant numerical tool, it has still some mesh related problems of mesh based methods. Some of the significant drawbacks of mesh based methods, especially for FEM, which were highlighted in literature [26,33,34,35] can be listed as follows:

- Mesh generation is a costly process and the most time consuming step in the simulation. It is not a fully automated process and human intervention is generally required especially for three dimensional cases.

- Finer meshes ,which eventually increase the computational cost, is generally required for the accurate representation of the boundaries of the problem domain and to obtain accurate results in problems with high gradients or a distinct local character.

- Severe distortion of elements in the simulation of problems including large geometry changes such as those in large deformation and shape optimization problem decreases the numerical accuracy considerably in mesh based methods. Mesh based methods are also not well suited to solve crack propagation problems where the arbitrary or complex paths of cracks must be modelled. Remeshing throughout the evolution of the problem is one way of dealing with these types of problems. To increase the numerical accuracy, meshing is repeated at each successive stage of the simulation so that severe distortion of elements is avoided and mesh lines remains coincident with any moving discontinuities. However, remeshing introduces some difficulties such as projection of field variables between meshes in each step and requires high computational cost especially for large three dimensional problems.

Dependence on a mesh can be seen the main cause of above drawbacks and then the first comes to mind as a solution is to eliminate the mesh.

1.1 Meshfree Methods

Meshfree methods, as the name implies, were developed to overcome the dependence on the mesh which is used to discretize the problem domain in mesh based methods and offer an alternative way of solving engineering problems without dealing with difficulties introduced by a mesh. In these methods, the approximate solution for partial differential is obtained using a set of scattered nodes without need an additional mesh. Meshfree methods represent the problem domain with arbitrarily distributed nodes in the problem domain and on its boundary. In the absence of a mesh, shape functions are constructed for particular points using the nodes in a small local domain, generally called the support domain, of the point. As the location of point changes, shape function changes. However, FEM uses element based shape functions and shape functions are the same for all the same type of elements. Meshfree methods use the same formulation principles as FEM to obtain a set of discrete system of equations. But, the procedure differs than FEM due to the difference in approximation technique of meshfree methods.

When compared to mesh based numerical methods, some of the advantages of meshfree methods highlighted in literature [26,33,34,35] can be listed as follows:

- The cost of mesh generation in the simulation is eliminated since the discretization is based on nodes in meshfree methods. Node generation is a rather simple process when compared to mesh generation process and can be performed fully automated manner by a computer.

- The absence of a mesh means that no connectivity information between nodes is needed before the simulation. Connectivity is defined during run as a part of computation.

- Adaptive analysis can be performed simply by adding nodes in the regions where a better accuracy is desired.

- Problems including large geometry changes which generally require remeshing in mesh based methods can be easily handled by changing the connectivity information with time.

- Boundaries of the problem can be represented accurately by meshfree discretization.

1.2 Literature Survey

Meshfree methods have attracted attention of researchers due to their distinctive properties and significant improvement has been achieved for the solution of partial differential equations in engineering problems so far. A group of these methods use collocation techniques to discretize the strong form of the governing differential equation to obtain the discrete system of equations. These methods are called meshfree strong form methods (or meshfree methods based on strong form). Another group, called meshfree weak form methods (or meshfree methods based on weak form), approximates the weak form of governing differential equations to form the discrete system equations. In the latter, weak form requires numerical integration globally or locally over the problem domain. First, to present the significant improvements in meshfree methods, a general survey of meshfree methods is given. Later, related to subject of the thesis, a survey about the usage of radial basis functions in meshfree methods is presented. As being older methods than meshfree weak form methods, an overview of meshfree strong form methods is given in general survey part first.

One of the oldest and famous meshfree methods is the smoothed particle hydrodynamics (SPH) which was introduced by Lucy [1] and Gingold, Monaghan [2] in 1977. They both used the SPH to model the astrophysical problems. It approximates the strong form of governing differential equation with kernel approximation which has a finite integral form.

Another mesh free strong form method is finite difference method at arbitrary irregular grids or generalized finite difference method (GFDM) which was proposed by Liszka and Orkisz [3] in 1980.

The finite point method (FPM) was proposed by Onate et al [4] in 1996. FPM is based on weighted least square interpolation of point data and point collocation technique for the evaluation of approximation integrals. It has been applied to fluid mechanics [5], [6] and elasticity problems [7].

In 1992, Nayroles et al [8] proposed diffuse element method (DEM) which is the first meshfree method based on weak form. They used in Galerkin weak form the moving least square (MLS) approximation. which was originated by mathematicians Lancaster and Salkauskas [9] for surface fitting in 1981. When compared to FEM, DEM has various advantages especially for evaluating the derivatives of unknown functions.

In 1994, Belytschko et al [10] further modified the DEM and developed the element free Galerkin method (EFGM). To improve numerical accuracy, they introduced several modifications in evaluation of the approximation derivatives, imposing the essential boundary conditions and numerical integration. EFGM has become a popular method and been applied to different classes of problems successfully.

The reproducing kernel particle method (RPKM) which was introduced by Liu et al [11] in 1995 is another example of meshfree method based on weak from. They added correction function to kernel approximations to improve the continuity in SPH. RPKM has the advantages of SPH and also gives much more accurate results due to addition of correction function. RPKM has also a strong form version proposed by Aluru [12] in 2000.

Duarte and Oden [13] and Babuska and Melenk [14] showed that methods based on MLS approximations are specific instances of partitions of unity (PU). Using the

PU concept, Babuska and Melenk [14] introduced the partition of unity finite element method (PUFEM). Duarte and Oden [13] proposed the Hp clouds method which is a meshfree weak form method based on h and p enrichment of the approximation functions in 1996.

In 1997, Mukherjee and Mukherjee [15] proposed the boundary node method (BNM) in which MLS approximations used in EFGM were combined with the boundary integral equations (BIE). The idea behind the BNM is to retain dimensionality advantage of BIE and meshfree property of MLS.

In 1998, Atluri and Zhu [16] introduced a truly meshfree method so called the meshless local Petrov-Galerkin method (MLPG) based on the local symmetric weak-form (LSWF) and MLS. The main idea for the development of the MLPG is to avoid the shadow elements needed for the evaluation of domain integrals in EFGM. In MLPG, integrals are evaluated only over regularly-shaped subdomains and their boundaries.

In 1999, Liu and Gu [17] proposed the point interpolation method (PIM) to replace the MLS approximation used for shape function construction in meshfree methods such as DEM, EFGM and MLG. The MLS approximation introduces some difficulties in the imposition of essential boundary conditions due to lack of Kronecker delta function property of the shape functions constructed. In PIM, shape functions have the Kronecker delta function property and simple forms when compared to the ones constructed with MLS. The original PIM was based on the Galerkin weak form and used polynomial PIM shape functions.

Improving and applying PIM to local Petrov-Galerkin formulation, the local point interpolation method (LPIM) was developed by Liu and Gu [18].

In 2002, Liu and Gu [23] proposed Meshfree weak-strong form (MWS) method which was based on the idea of combining the strong form and local weak form to

develop a truly meshfree method. For the nodes on the natural boundaries, the local weak form is used and for the rest of the nodes, strong form is used. So, the nodes on the natural boundaries only requires numerical integration. It is more accurate and stable than meshfree strong form methods and more efficient than meshfree weak form methods.

In 1990, multiquadric radial basis functions were first used by Kansa [25] to solve partial differential equations. Approximations based on radial basis functions were used in meshfree methods also by other researchers, one example is radial basis functions used in MLPG approaches for the solutions of three dimensional elasticity problems by Han and Atluri [28].

PIM with polynomial basis function suffers from the singularity of moment matrix in the interpolation. To guarantee non-singular moment matrix, some special techniques proposed in PIM. Matrix triangularization algorithm (MTA) which was developed by Liu and Gu [20] is one of these techniques. Another technique is the introduction of radial functions as the basis. Wang and Liu [19] replaced the polynomial basis functions in PIM with radial basis functions and developed the radial point interpolation method (RPIM). The RPIM was also applied to local Petrov-Galerkin formulation and the local radial point interpolation method (LRPIM) was developed by Liu and Gu [21] in 2001. Combining with boundary integral equation, boundary types of PIM and RPIM was also formulated as the boundary point interpolation method (BPIM) and the boundary radial point interpolation method (BRPIM) respectively by Liu GR and Gu [22].

Wang and Liu [31] and Liu and Gu [32] investigated the effect of shape parameters of radial basis functions in two dimensional meshfree methods and recomended some optimal shape parameters.

1.3 Objective and Scope of the Study

The main objective of this study is to implement the radial point interpolation method (RPIM) as a meshfree method to analyze plane elasticity problems and to study the effect of shape parameters of radial basis functions on the accuracy of RPIM. To this end, a computer code implementing RPIM with multiquadric (MQ) basis functions has been developed for the solution of plane elasticity problems. Problems whose analytical solutions are available in literature have been selected and solved with developed code. The effect of shape parameters on the accuracy has been studied through stress error analysis and the optimal shape parameters of MQ radial basis functions have been determined to achieve the best accuracy for plane elasticity problems.

Thesis report is organized as follows:

- In Chapter 2, a brief information about plane elasticity is provided and the relevant equations for plane elasticity for the formulation of RPIM are presented.

- In Chapter 3, domain representation, shape function construction method, formulation, numerical integration, imposition of essential boundary conditions and general procedure in the RPIM are described.

- In Chapter 4, for several problems, numerical results of stress error analysis study on the accuracy of the RPIM for different shape parameters and discussions of results are presented.

- In Chapter 5, conclusions drawn according to results obtained in Chapter 4 are provided.

CHAPTER 2

PLANE ELASTICITY

Under the action external forces, solids and structures made of solids deform. Depending on the material property, this deformation can disappear and initial form can be recovered. Elasticity is the property of a structural material to return its initial undeformed form completely after removal of external forces acting on it. In this deformation, the rate of displacement at a point in the solid is called strain. Internal forces are introduced in the solid, to balance the external forces. Magnitude of these forces are defined by their intensities. This intensity is called stress. Elasticity theory establishes mathematical model to determine the stress, strain and displacement distribution in elastic solid under the action of external forces.

In many cases, materials display a behaviour such that the stress and strain vary proportionally up to a limit. This behaviour is called linearly elastic behaviour and the limit is called proportional limit.

Materials can be anisotropic or isotropic depending on the variation of material property with direction. Material displaying direction-dependent properties is called anisotropic. If the material properties are identical in all directions at a point, then the material is called isotropic.

It is not an efficient way to solve all real problems using governing elasticity field equations developed for three-dimensional problems. Simplified formulations have been developed taking the advantages related to geometry, loading and boundary

conditions. Plane elasticity is a special case where a three dimensional problem is simplified to one involving two dimensions only.

In this thesis, plane elasticity problems for linearly elastic and isotropic are considered therefore the relevant information will be given further in this chapter for the formulation of radial point interpolation method.

There are two basic cases of plane elasticity. One is the plane stress and the other is plane strain. If a plate whose thickness in z direction is very small in comparison to the dimensions in other directions is loaded by forces acting in the plane of the plate and uniformly distributed over the thickness as seen in Figure 2-1, the stresses in z direction are all zero. The state of stress is then specified by σ_x, σ_y, τ_{xy} only and called the plane stress. These components are functions of x and y only. A similar simplification can be obtained for the state of strain also. Consider an infinitely long cylindrical or prismatic body subjected to the load laterally as seen in Figure 2-2. Assuming the load to be function of x and y only, all the sections experience the same deformation and therefore the strain components in the z direction are all zero. This deformation state is referred to as plain strain.

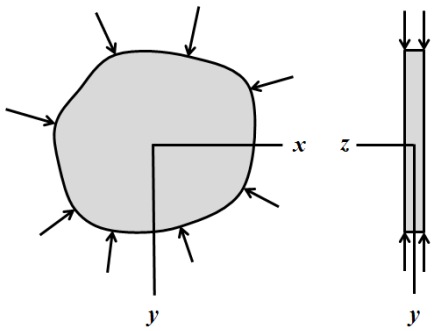

Figure 2-1 Plane stress case

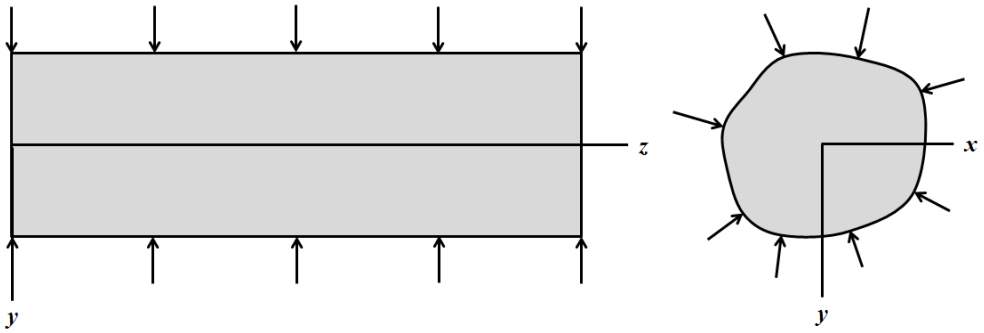

Figure 2-2 Plane strain case

2.1 Equations for Plane Elasticity

After simplifications, the relevant equations left for plane elasticity are the followings.

The displacements are given as

$$\mathbf{u} = \begin{bmatrix} u & v \end{bmatrix}^T \tag{2.1}$$

The stress components in vector notation are expressed as

$$\boldsymbol{\sigma} = \begin{bmatrix} \sigma_x & \sigma_y & \tau_{xy} \end{bmatrix}^T \tag{2.2}$$

The strain components in vector notation expressed as

$$\boldsymbol{\varepsilon} = \begin{bmatrix} \varepsilon_x & \varepsilon_y & \varepsilon_{xy} \end{bmatrix}^T \tag{2.3}$$

The strain-displacement relationships can be written as

$$\varepsilon_{xx} = \frac{\partial u}{\partial x} \qquad \varepsilon_{yy} = \frac{\partial v}{\partial y} \qquad \varepsilon_{xy} = \frac{\partial u}{\partial y} + \frac{\partial v}{\partial x} \tag{2.4}$$

or in matrix notation

$$\boldsymbol{\varepsilon} = \mathbf{L}\mathbf{u} \tag{2.5}$$

where the differential operator **L** is expressed as

$$\mathbf{L} = \begin{bmatrix} \dfrac{\partial}{\partial x} & 0 \\ 0 & \dfrac{\partial}{\partial y} \\ \dfrac{\partial}{\partial y} & \dfrac{\partial}{\partial x} \end{bmatrix} \tag{2.6}$$

The linear stress-strain relationship in the matrix notation is expressed as

$$\boldsymbol{\sigma} = \mathbf{D}\boldsymbol{\varepsilon} \tag{2.7}$$

where matrix **D** for isotropic material in the plane stress case is given by

$$\mathbf{D} = \frac{E}{1-\upsilon^2}\begin{bmatrix} 1 & \upsilon & 0 \\ \upsilon & 1 & 0 \\ 0 & 0 & \dfrac{1-\upsilon}{2} \end{bmatrix} \tag{2.8}$$

for isotropic material in the plane strain case is given by

$$\mathbf{D} = \frac{E}{(1+\upsilon)(1-2\upsilon)}\begin{bmatrix} 1-\upsilon & \upsilon & 0 \\ \upsilon & 1 & 0 \\ 0 & 0 & \dfrac{1-2\upsilon}{2} \end{bmatrix} \tag{2.9}$$

Equations of equilibrium for static problem are expressed as

$$\frac{\partial \sigma_x}{\partial x} + \frac{\partial \tau_{xy}}{\partial y} + b_x = 0$$
$$\frac{\partial \sigma_y}{\partial y} + \frac{\partial \tau_{xy}}{\partial x} + b_y = 0 \qquad (2.10)$$

or in matrix notation

$$\mathbf{L}^T \boldsymbol{\sigma} + \mathbf{b} = \mathbf{0} \qquad (2.11)$$

where the body force vector **b** is given by

$$\mathbf{b} = \begin{Bmatrix} b_x \\ b_y \end{Bmatrix} \qquad (2.12)$$

The natural and essential boundary conditions can be expressed respectively as

$\boldsymbol{\sigma}\mathbf{n} = \bar{\mathbf{t}}$ on the natural boundary Γ_t (2.13)

$\mathbf{u} = \bar{\mathbf{u}}$ on the essential boundary Γ_u (2.14)

where $\bar{\mathbf{t}}$ is the vector of prescribed surface tractions on the natural boundary Γ_t and given by

$$\bar{\mathbf{t}} = \begin{bmatrix} \bar{t}_x & \bar{t}_y \end{bmatrix}^T \qquad (2.15)$$

n is the unit outward normal vector on the boundary Γ and $\bar{\mathbf{u}}$ is the vector of prescribed displacements on the essential boundary Γ_u and given by

$$\bar{\mathbf{u}} = \begin{bmatrix} \bar{u} & \bar{v} \end{bmatrix}^T \qquad (2.16)$$

CHAPTER 3

RADIAL POINT INTERPOLATION METHOD

Point interpolation method (PIM) was first offered by Liu and Gu [17] in 1999 as an alternative shape function construction method to moving least squares (MLS) used in EFGM. In PIM, approximation is constructed in a way that interpolation function satisfies the values of variables at field nodes in the support domain. So, different then MLS, shape functions constructed with PIM possesses the Kronecker delta function property meaning that the essential boundary conditions can be imposed easily. PIM uses Galerkin weak form to obtain discrete system equations. Evaluation of the integrals in weak form requires to use a quadrature integration scheme. In PIM, integration is performed using Gauss quadrature with a background mesh.

Original PIM uses polynomials as basis functions, radial point interpolation method (RPIM) is a type of PIM where radial basis functions are introduced as basis to avoid a non-singular moment matrix in the construction of approximation.

This chapter presents the general procedure of RPIM including domain representation, construction of shape functions, formulation of RPIM, evaluation of integrals and imposition of essential boundary conditions.

3.1 Domain Representation

Since the approximation is constructed in terms of nodes in RPIM as in all meshfree methods, the first step is representation of the problem domain with nodes. PIM represents the problem domain with a set of arbitrarily distributed nodes in the problem domain and on its boundary as seen in Figure 3-1.

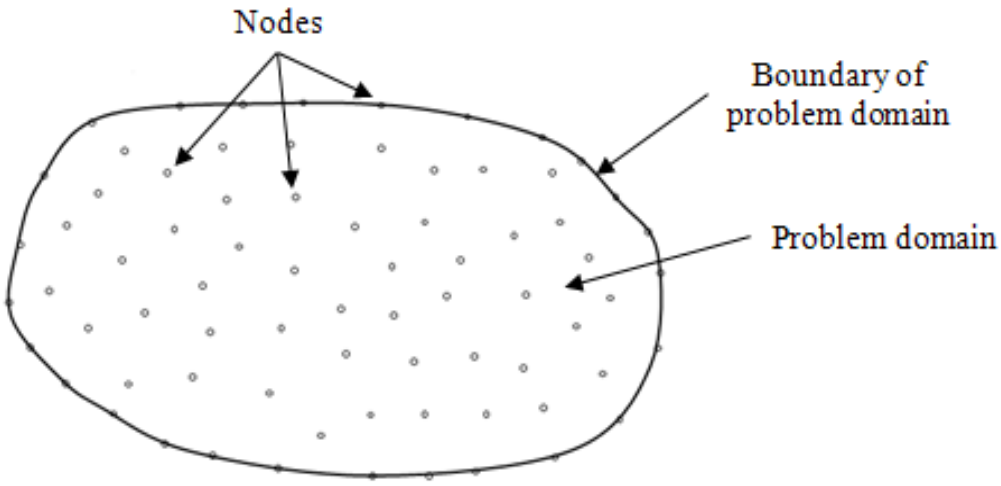

Figure 3-1 Domain representation

In this thesis, for problems having simple geometries nodes are generated by simply inputting the coordinates of the nodes. For problems having relatively complex geometries, node generation is performed using MSC Patran. First, solid body of the problem is modelled then mesh of finite elements is created. Then just using the nodes and discarding the elements, nodal representation of the problem domain and its boundaries is obtained.

3.2 Construction of Shape Functions

Liu [26] classified point interpolation method (PIM) as a finite series representation method for the function approximation. PIM interpolates the field variables by enforcing the interpolation function pass through the function values at each scattered node within the defined support of domain.

The number of surrounding nodes to interpolate the function value at a point is determined by the support domain of the point. In this thesis, circular support domains (see Figure 3-2) are used and a fixed number of nodes is used in the support domain of each point.

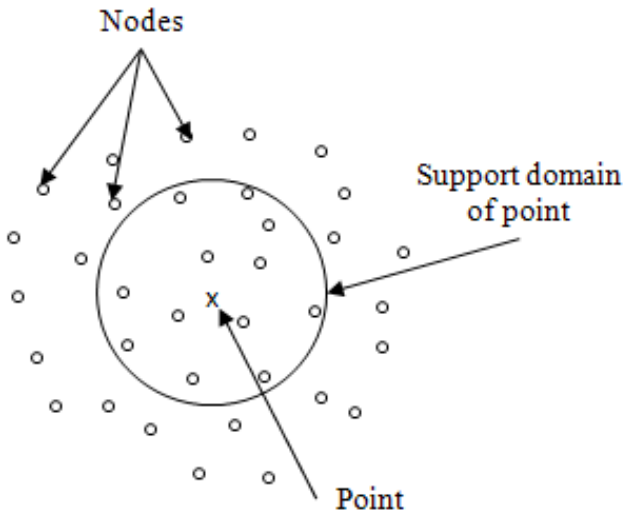

Figure 3-2 Support domain of a point

Let $u(\mathbf{x})$ be field variable function defined in the problem domain. The domain is represented by a set of arbitrarily distributed nodes in the problem domain and its boundary. In PIM, approximation for the function $u(\mathbf{x})$ within a support domain at point $\mathbf{x}$ is given by

$$u(\mathbf{x}) = \sum_{i=1}^{n} B_i(\mathbf{x}) a_i \tag{3.1}$$

where $B_i(\mathbf{x})$ are basis functions defined in spatial coordinates $\mathbf{x}^T=[x, y]$ for two dimensional problems, n is the number of the surrounding nodes in the support domain of point $\mathbf{x}$ and a_i are the coefficients of the basis functions $B_i(\mathbf{x})$.

Liu and Gu [17] first used polynomial functions as basis functions. Using polynomial basis functions may result a non-singular moment matrix in the shape function construction. Some techniques have been proposed to avoid a non singular moment matrix. One of these techniques is to use radial basis function proposed by Wang and Liu [19] in the function approximation.

Choosing radial basis functions as the basis, Equation 3.1 is written as

$$u(\mathbf{x}) = \sum_{i=1}^{n} R_i(\mathbf{x}) a_i \tag{3.2}$$

where $R_i(\mathbf{x})$ are the radial basis functions defined in spatial coordinates $\mathbf{x}^T=[x, y]$ for two dimensional problems. In the radial basis function $R_i(\mathbf{x})$, the variable is the distance r between the point of interest $\mathbf{x}$ and a node at $\mathbf{x}_i$. For two dimensional case, r is expressed as:

$$r = \sqrt{(x - x_i)^2 + (y - y_i)^2} \tag{3.3}$$

Multiquadric (MQ), Gaussian, thin plate spline and logarithmic radial basis functions are often used radial basis functions. In this thesis, only MQ radial basis functions will be considered. MQ radial basis function is given by,

$$R_i(x, y) = \left(r_i^2 + C^2\right)^q \tag{3.4}$$

where q and C are shape parameters. Dimensionless formulation of MQ radial basis functions has the form [26].

$$R_i(x,y)=\left(r_i^2+(cd_c)^2\right)^q \tag{3.5}$$

where c is the dimensionless shape parameter and d_c is the average nodal spacing in the local support domain of point **x**.

The consistency of shape function is defined as the ability to reproduce the complete order of polynomial. The RPIM shape functions are not consistent i.e., they can not reproduce linear field function exactly. Wang and Liu [24] proposed to use radial basis function with polynomial basis functions up to linear orders to ensure the consistency of RPIM shape functions.

Adding polynomials basis functions, Equation 3.2 becomes

$$u(\mathbf{x})=\sum_{i=1}^{n}R_i(\mathbf{x})a_i+\sum_{j=1}^{m}p_j(\mathbf{x})b_j \tag{3.6}$$

where $p_j(\mathbf{x})$ are the monomials in spatial coordinates $\mathbf{x}^{\mathrm{T}}=[x, y]$ for two dimensional problems, m is the number of polynomial basis functions and b_j are the corresponding coefficients for the polynomial basis functions $p_j(\mathbf{x})$.

Equation 3.6 can be written in the matrix form as

$$u(\mathbf{x})=\mathbf{R}^{\mathrm{T}}(\mathbf{x})\mathbf{a}+\mathbf{p}^{\mathrm{T}}(\mathbf{x})\mathbf{b} \tag{3.7}$$

where the vector **R** of radial basis functions has the form

$$\mathbf{R}^{\mathrm{T}}(\mathbf{x})=\left[R_1(\mathbf{x}),R_2(\mathbf{x}),.....,R_n(\mathbf{x})\right] \tag{3.8}$$

the vector **p** of polynomial terms has the form

$$\mathbf{p}^{\mathrm{T}}(\mathbf{x}) = \left[p_1(\mathbf{x}), p_2(\mathbf{x}), ..., p_m(\mathbf{x})\right] \tag{3.9}$$

the vector **a** is written as

$$\mathbf{a}^{\mathrm{T}} = \left[a_1, a_2, ..., a_n\right] \tag{3.10}$$

and the vector **b** is written as

$$\mathbf{b}^{\mathrm{T}} = \left[b_1, b_2, ..., b_m\right] \tag{3.11}$$

One may determine, the coefficients a_i and b_j by enforcing interpolation function $u(\mathbf{x})$ satisfy the nodal values at n surrounding nodes in the support domain of point **x.** Therefore, at each node, we have

$$u_i = \mathbf{R}^{\mathrm{T}}(x_i)\mathbf{a} + \mathbf{p}^{\mathrm{T}}(x_i)\mathbf{b} \tag{3.12}$$

Equation 3.12 can be written in the matrix form as

$$\mathbf{U}_s = \mathbf{R}_0\mathbf{a} + \mathbf{P}_m\mathbf{b} \tag{3.13}$$

where the vector $\mathbf{U}_s$ is

$$\mathbf{U}_s^{\mathrm{T}} = \left[u_1 \quad u_2 \quad . \quad . \quad . \quad u_n\right] \tag{3.14}$$

the moment matrix of radial basis functions, $\mathbf{R}_0$ is expressed as

$$\mathbf{R}_0 = \begin{bmatrix} R_1(r_1) & R_2(r_1) & . & . & R_n(r_1) \\ R_1(r_2) & R_2(r_2) & . & . & R_n(r_2) \\ . & . & . & & . \\ . & . & & . & . \\ R_1(r_n) & R_2(r_n) & . & . & R_n(r_n) \end{bmatrix} \tag{3.15}$$

the moment matrix of polynomial terms $\mathbf{P}_m$ is expressed as

$$\mathbf{P}_m = \begin{bmatrix} 1 & x_1 & . & . & p_m(x_1) \\ 1 & x_2 & . & . & p_m(x_2) \\ . & . & . & & . \\ . & . & & . & . \\ 1 & x_n & . & . & p_m(x_n) \end{bmatrix} \tag{3.16}$$

In order to have an unique solution, the following constraints are imposed for the polynomial terms

$$\sum_i^m p_j(\mathbf{x}_i) a_i = 0 \qquad j = 1, 2, ..., m \tag{3.17}$$

or in matrix form

$$\mathbf{P}_m^T \mathbf{a} = \mathbf{0} \tag{3.18}$$

Combining Equations 3.13 and 3.18, the following equation is obtained

$$\begin{bmatrix} \mathbf{R}_0 & \mathbf{P}_m \\ \mathbf{P}_m^T & \mathbf{0} \end{bmatrix} \begin{bmatrix} \mathbf{a} \\ \mathbf{b} \end{bmatrix} = \begin{bmatrix} \mathbf{U}_s \\ \mathbf{0} \end{bmatrix} \tag{3.19}$$

or

$$\mathbf{G}\begin{bmatrix}\mathbf{a}\\ \mathbf{b}\end{bmatrix}=\begin{bmatrix}\mathbf{U}_s\\ \mathbf{0}\end{bmatrix} \tag{3.20}$$

Solving Equation 3.20, we have

$$\begin{bmatrix}\mathbf{a}\\ \mathbf{b}\end{bmatrix}=\mathbf{G}^{-1}\begin{bmatrix}\mathbf{U}_s\\ \mathbf{0}\end{bmatrix} \tag{3.21}$$

Equation 3.7 can be re-written as

$$u(\mathbf{x})=\mathbf{R}^{\mathrm{T}}(\mathbf{x})\mathbf{a}+\mathbf{p}^{\mathrm{T}}(\mathbf{x})\mathbf{b}=\begin{bmatrix}\mathbf{R}^{\mathrm{T}}(\mathbf{x}) & \mathbf{p}^{\mathrm{T}}(\mathbf{x})\end{bmatrix}\begin{bmatrix}\mathbf{a}\\ \mathbf{b}\end{bmatrix} \tag{3.22}$$

Substituting Equation 3.21 into Equation 3.22 gives

$$u(\mathbf{x})=\begin{bmatrix}\mathbf{R}^{\mathrm{T}}(\mathbf{x}) & \mathbf{p}^{\mathrm{T}}(\mathbf{x})\end{bmatrix}\mathbf{G}^{-1}\begin{bmatrix}\mathbf{U}_s\\ \mathbf{0}\end{bmatrix}=\widetilde{\mathbf{\Phi}}^{\mathrm{T}}\begin{bmatrix}\mathbf{U}_s\\ \mathbf{0}\end{bmatrix} \tag{3.23}$$

where the RPIM shape functions are expressed as

$$\begin{aligned}\widetilde{\mathbf{\Phi}}^{\mathrm{T}}&=\begin{bmatrix}\mathbf{R}^{\mathrm{T}}(\mathbf{x}) & \mathbf{p}^{\mathrm{T}}(\mathbf{x})\end{bmatrix}\mathbf{G}^{-1}\\ &=\begin{bmatrix}\Phi_1(\mathbf{x}) & \Phi_1(\mathbf{x}) & . & . & \Phi_n(\mathbf{x}) & \Phi_{n+1}(\mathbf{x}) & \Phi_{n+2}(\mathbf{x}) & . & . & \Phi_{n+m}(\mathbf{x})\end{bmatrix}\end{aligned} \tag{3.24}$$

The RPIM shape functions corresponding to nodal variables are expressed as

$$\mathbf{\Phi}^{\mathrm{T}}=\begin{bmatrix}\Phi_1(\mathbf{x}) & \Phi_2(\mathbf{x}) & . & . & \Phi_n(\mathbf{x})\end{bmatrix} \tag{3.25}$$

Equation 3.23 can be written as

$$u(\mathbf{x})=\sum_{i=1}^{n}\Phi_i(x)u_i \tag{3.26}$$

3.3 RPIM Formulation

A plane elasticity problem can be defined with the equilibrium equation given by Equation 2.11 in the global domain Ω as

$$\mathbf{L}^T\boldsymbol{\sigma}+\mathbf{b}=\mathbf{0} \qquad \text{in } \Omega \tag{3.27}$$

where **L**, **σ** and **b** are given by Equations 2.6, 2.7 and 2.12 respectively

and with the natural and essential boundary conditions given by Equation 2.13 on the natural boundary Γ_t and Equation 2.14 on the essential boundary Γ_u respectively as

$$\boldsymbol{\sigma}\mathbf{n}=\bar{\mathbf{t}} \qquad \text{on } \Gamma_t \tag{3.28}$$

$$\mathbf{u}=\bar{\mathbf{u}} \qquad \text{on } \Gamma_u \tag{3.29}$$

where **n** is the unit outward normal vector on the boundary Γ and $\bar{\mathbf{t}}$, **u** and $\bar{\mathbf{u}}$ are given by Equations 2.15, 2.1 and 2.16.

The displacements *u* and *v* can be written with the approximation 3.26 as

$$u(\mathbf{x})=\sum_{i=1}^{n}\Phi_i(x)u_i \tag{3.30}$$

$$v(\mathbf{x})=\sum_{i=1}^{n}\Phi_i(x)v_i \tag{3.31}$$

Combining Equations 3.30 and 3.31, we have

$$\mathbf{u}=\begin{bmatrix}u(\mathbf{x})\\ v(\mathbf{x})\end{bmatrix}=\sum_{i=1}^{n}\begin{bmatrix}\Phi_i & 0\\ 0 & \Phi_i\end{bmatrix}\begin{bmatrix}u_i\\ v_i\end{bmatrix}=\sum_{i=1}^{n}\boldsymbol{\Phi}_i\mathbf{u}_i \tag{3.32}$$

Substitution of Equation 3.32 into strain-displacement relationship given by Equation 2.5 yields

$$\boldsymbol{\varepsilon} = \mathbf{L}\mathbf{u} = \mathbf{L}\sum_{i=1}^{n} \boldsymbol{\Phi}_i \mathbf{u}_i = \sum_{i=1}^{n} \mathbf{L}\boldsymbol{\Phi}_i \mathbf{u}_i = \sum_{i=1}^{n} \mathbf{B}_i \mathbf{u}_i \tag{3.33}$$

where

$$\mathbf{B}_i = \begin{bmatrix} \dfrac{\partial}{\partial x} & 0 \\ 0 & \dfrac{\partial}{\partial y} \\ \dfrac{\partial}{\partial y} & \dfrac{\partial}{\partial x} \end{bmatrix} \begin{bmatrix} \Phi_i & 0 \\ 0 & \Phi_i \end{bmatrix} = \begin{bmatrix} \Phi_{i,x} & 0 \\ 0 & \Phi_{i,y} \\ \Phi_{i,y} & \Phi_{i,x} \end{bmatrix} \tag{3.34}$$

Substituting Equation 3.33 into stress-strain relationship given by Equation 2.7, we have

$$\boldsymbol{\sigma} = \mathbf{D}\boldsymbol{\varepsilon} = \mathbf{D}\sum_{I}^{n} \mathbf{B}_I \mathbf{u}_I = \sum_{I}^{n} \mathbf{D}\mathbf{B}_I \mathbf{u}_I \tag{3.35}$$

The Galerkin weak-form for the plane elasticity defined by Equations 3.27, 3.28 and 3.29 can be written using virtual work principle as

$$\int_{\Omega} \delta\boldsymbol{\varepsilon}^{\mathrm{T}} \boldsymbol{\sigma} \mathrm{d}\Omega - \int_{\Omega} \delta\mathbf{u}^{\mathrm{T}} \mathbf{b} \mathrm{d}\Omega - \int_{\Gamma_t} \delta\mathbf{u}^{\mathrm{T}} \bar{\mathbf{t}} \mathrm{d}\Gamma = \mathbf{0} \tag{3.36}$$

where the first term is work done by internal force, the second term is work done by body force and the last term is work done by external force.

Substituting Equations 3.32, 3.33 and 3.35 into equation 3.36 final discrete system equations can be obtained as follows

$$\int_{\Omega} \delta\left(\sum_{i=1}^{n} \mathbf{B}_i \mathbf{u}_i\right)^{\mathrm{T}} \left(\sum_{j=1}^{n} \mathbf{D}\mathbf{B}_j \mathbf{u}_j\right) \mathrm{d}\Omega - \int_{\Omega} \delta\left(\sum_{i=1}^{n} \boldsymbol{\Phi}_i \mathbf{u}_i\right)^{\mathrm{T}} \mathbf{b} \mathrm{d}\Omega - \int_{\Gamma_t} \delta\left(\sum_{i=1}^{n} \boldsymbol{\Phi}_i \mathbf{u}_i\right)^{\mathrm{T}} \bar{\mathbf{t}} \mathrm{d}\Gamma = \mathbf{0} \tag{3.37}$$

$$\sum_{i=1}^{n}\sum_{j=1}^{n}\partial\mathbf{u}_I^{\mathrm{T}}\left(\int_{\Omega}\mathbf{B}_i^{\mathrm{T}}\mathbf{D}\mathbf{B}_j\mathrm{d}\Omega\right)\mathbf{u}_J-\sum_{i=1}^{n}\partial\mathbf{u}_i^{\mathrm{T}}\int_{\Omega}\boldsymbol{\Phi}_i^{\mathrm{T}}\mathbf{b}\mathrm{d}\Omega-\sum_{i=1}^{n}\partial\mathbf{u}_i^{\mathrm{T}}\int_{\Gamma_t}\boldsymbol{\Phi}_i^{\mathrm{T}}\bar{\mathbf{t}}\mathrm{d}\Omega=\mathbf{0} \tag{3.38}$$

n covers the nodes in the local support domain, to include all nodes in the problem domain, summation limits must be changed from *n* to *N* which is the total number of nodes in the problem domain.

$$\sum_{i=1}^{N}\sum_{j=1}^{N}\partial\mathbf{u}_I^{\mathrm{T}}\mathbf{K}_{ij}\mathbf{u}_J-\sum_{i=1}^{N}\partial\mathbf{u}_i^{\mathrm{T}}\mathbf{f}_i^b-\sum_{i=1}^{N}\partial\mathbf{u}_i^{\mathrm{T}}\mathbf{f}_i^t=\mathbf{0} \tag{3.39}$$

where $\mathbf{K}_{ij}$ is the nodal stiffness matrix in the form of

$$\mathbf{K}_{ij}=\int_{\Omega}\mathbf{B}_i^{\mathrm{T}}\mathbf{D}\mathbf{B}_j\mathrm{d}\Omega \tag{3.40}$$

$\mathbf{f}_i^b$ is the nodal body force vector in the form of

$$\mathbf{f}_i^b=\int_{\Omega}\boldsymbol{\Phi}_i^{\mathrm{T}}\mathbf{b}\mathrm{d}\Omega \tag{3.41}$$

and $\mathbf{f}_i^t$ is the nodal traction force vector in the form of

$$\mathbf{f}_i^t=\int_{\Gamma_t}\boldsymbol{\Phi}_i^{\mathrm{T}}\bar{\mathbf{t}}\mathrm{d}\Omega \tag{3.42}$$

Equation 3.39 can further be written as

$$\partial\mathbf{U}^{\mathrm{T}}\mathbf{K}\mathbf{U}-\partial\mathbf{U}^{\mathrm{T}}\mathbf{F}^b-\partial\mathbf{U}^{\mathrm{T}}\mathbf{F}^t=\mathbf{0} \tag{3.43}$$

$$\partial \mathbf{U}^{\mathrm{T}} \left(\mathbf{KU} - \mathbf{F}^{b} - \mathbf{F}^{t} \right) = \mathbf{0} \tag{3.44}$$

where **U** is the global displacement vector, **K** is global stiffness matrix which is assembled using $\mathbf{K}_{ij}$, $\mathbf{F}^{b}$ is the global body force vector which is assembled using $\mathbf{f}_{i}^{b}$ and $\mathbf{F}^{t}$ is the global traction force vector which is assembled using $\mathbf{f}_{i}^{t}$. Equation 3.44 can be satisfied only if

$$\mathbf{KU} - \mathbf{F}^{b} - \mathbf{F}^{t} = \mathbf{0} \tag{3.45}$$

Finally, writing the global body force vector $\mathbf{F}^{b}$ and the global traction force vector $\mathbf{F}^{t}$ together as the global force vector **F**, the final discrete system equation can be obtained as

$$\mathbf{KU} - \mathbf{F} = \mathbf{0} \tag{3.46}$$

$$\mathbf{KU} = \mathbf{F} \tag{3.47}$$

3.4 Evaluation of Integrals

Formulation of RPIM for a plane elasticity problem is presented in Section 3.3 through the use of Galerkin weak form to obtain discrete system equations. As all other meshfree methods based Galerkin weak form, RPIM requires a quadrature integration scheme to evaluate the integrals in the weak form. Two area integrals in Equations 3.40 and 3.41 and one line integral in Equation 3.42 appear in the steps of formulation. RPIM uses Gauss quadrature to evaluate these integrals numerically with a background mesh. This can be seen a disadvantage of RPIM and the requirement of a mesh for integration makes impossible to see the method as a truly meshfree method. However, background mesh is used just for integration and independent of the nodes used to construct approximation for the field variables.

From this point of view, RPIM can be seen as meshfree in terms of approximation of field variables only. Different than the mesh in FEM which is used for both approximation and numerical integration, a suitable background mesh to ensure a numerical integration of desired accuracy is enough in RPIM.

In this thesis, quadrilateral background mesh is used for the numerical integration in the studied problems. For problems with simple geometry, background mesh is defined by entering the coordinates of corner points of quadrilateral elements and defining the connectivity information in between the elements. For complex geometries studied, a background mesh is generated using MSC Patran.

3.5 Imposition of Essential Boundary Conditions

In Meshfree methods using MLS method for the shape function construction, imposition of essential boundary conditions requires special techniques due to the fact that approximation does not satisfy the values of variables at field nodes. However, in PIM and also RPIM, shape functions constructed possesses the Kronecker delta function property i.e., the approximation satisfies the values of variables at field nodes. This property of the shape function RPIM enables easy imposition of essential boundary conditions as in FEM, so no special treatment is required.

3.6 RPIM Procedure

Implementation of RPIM for a plane elasticity problem can be realized according to the following step by step procedure:

1. Model the geometry of the problem.

2. Generate a finite number of nodes to represent the problem domain and its boundaries.

3. Generate a background mesh and Gauss points for the numerical integration for Gauss quadrature.

4. Determine the nodes to support the approximation at each Gauss point.

5. Create shape functions $\mathbf{\Phi}_i$ and its derivatives $\mathbf{B}_i$ for the nodes in the support domain of each Gauss point.

6. Perform numerical integration to find the contribution of each Gauss point in the problem domain to nodal stiffness matrices $\mathbf{K}_{ij}$ and nodal body force vector $\mathbf{f}_i^b$ and to find the contribution of each Gauss point on the problem domain boundary to nodal traction force vector $\mathbf{f}_i^t$.

7. Form the global stiffness matrix $\mathbf{K}$ by assembling the nodal stiffness matrices $\mathbf{K}_{ij}$ and global force vector $\mathbf{F}$ by assembling the nodal force vectors $\mathbf{f}_i^b$ and $\mathbf{f}_i^t$.

8. Solve linear system equation to find the displacements $\mathbf{U}$ at all nodes.

9. Calculate stress and strain at all nodes.

CHAPTER 4

NUMERICAL EXAMPLES AND DISCUSSION

A computer code implementing RPIM with multiquadric (MQ) radial basis functions for the solution of plane elasticity problems is developed using Fortran programming language. In this chapter, a number of plane elasticity problems is solved with the code to illustrate the performance of RPIM and the effect of shape parameters (c, q) of MQ radial basis functions on the accuracy of RPIM is studied through stress error analysis. Problems whose analytical solutions are available in the literature are selected for accurate error analysis. Selected problems includes cantilever beam loaded at the end, infinite plate with circular hole under uniform far-field load, thick-walled hollow cylinder under uniform internal pressure and curved beam loaded at the end. Meshfree models of the problems are defined and suitable background meshes are applied for accurate numerical integration. Each problem is solved for a range of values of c and q with and without polynomial terms added in the interpolation and to illustrate the effect of shape parameters on the numerical accuracy, error values are plotted for different values c and q. In all studied problems, linear basis functions (m=3) added as polynomial terms. Numerical results of error analysis are discussed for each problem and the optimal shape parameters common to all problems are determined. Deflection and stress plots with the optimal shape parameters are also presented.

For the purpose of error analysis, a relative percentage of stress error is defined as

$$\eta = 100 * \frac{\|e\|}{\|\varphi\|} \tag{4.1}$$

where $\|e\|$ and $\|\varphi\|$ are given by

$$\|e\| = \left[\int_{\Omega} \left(\boldsymbol{\sigma}^{num} - \boldsymbol{\sigma}^{exact} \right)^T \left(\boldsymbol{\sigma}^{num} - \boldsymbol{\sigma}^{exact} \right) \right]^{\frac{1}{2}} \tag{4.2}$$

$$\|\varphi\| = \left[\int_{\Omega} \boldsymbol{\sigma}^{exact^T} \boldsymbol{\sigma}^{exact} \right]^{\frac{1}{2}} \tag{4.3}$$

4.1 Cantilever Beam Loaded at the End

The problem of a cantilever beam having a narrow rectangular cross section of unit width with a load P at the end is shown in Figure 4-1. End load is distributed parabolically along the end and has a resultant of P.

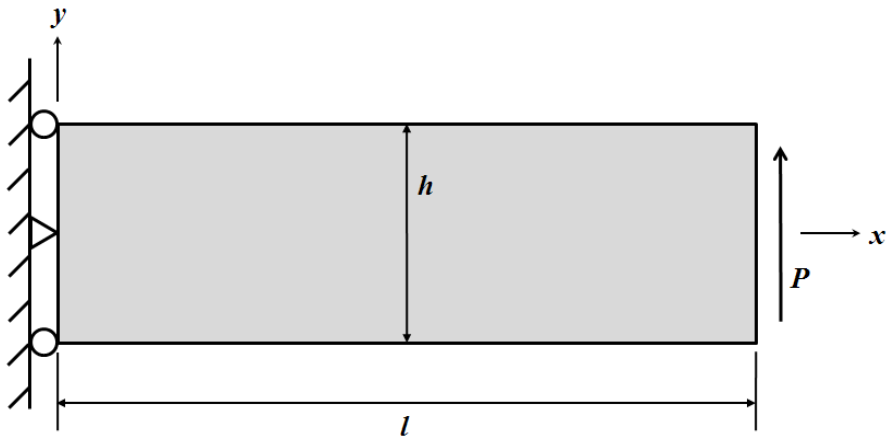

Figure 4-1 Cantilever beam loaded at the end

Analytical solution of the problem is given as follows [30].

The displacement component in x direction is

$$u = -\frac{Py}{6EI}\left[(6l-3x)x+(2+\upsilon)\left[y^2-\frac{h^2}{4}\right]\right] \tag{4.4}$$

The displacement component in y direction is

$$v = \frac{P}{6EI}\left[3\upsilon y^2(l-x)+(4+5\upsilon)\frac{h^2x}{4}+(3l-x)x^2\right] \tag{4.5}$$

where moment of inertia is given by

$$I = \frac{h^3}{12} \tag{4.6}$$

The normal stress component in x direction is

$$\sigma_x = -\frac{P(l-x)y}{I} \tag{4.7}$$

The normal stress component in y direction is

$$\sigma_y = 0 \tag{4.8}$$

The shear stress is

$$\tau_{xy} = \frac{P}{2I}\left(\frac{h^2}{4} - y^2\right) \tag{4.9}$$

Analytical displacement solutions given by Equations 4.4 and 4.5 are prescribed at the left end in numerical model. Parabolic end load is distributed according to Equation 4.9 at right end.

Parameters for this problem are chosen as in Table 4-1.

Table 4-1 Parameters for the problem of cantilever beam loaded at the end

Parameter	Value
Load, P	-500 N
Young's modulus, E	30000000 N/mm^2
Poisson's ratio, υ	0.3
Height, h	18 mm
Length, l	90 mm

The problem is solved for plane stress case. The domain of cantilever beam is modelled using 217 regularly distributed field nodes as shown in Figure 4-2. A background mesh of 80 rectangular cells as shown in Figure 4-3 are used for numerical integration. 4*4 Gauss points are used in each cell. Circular support domains are defined and fixed number (30) of nodes is used in support domain of each Gauss point for displacement interpolation.

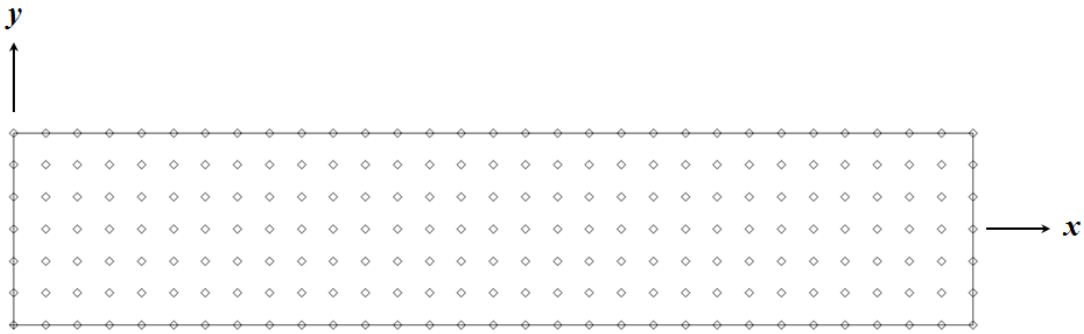

Figure 4-2 Node distribution for cantilever beam problem

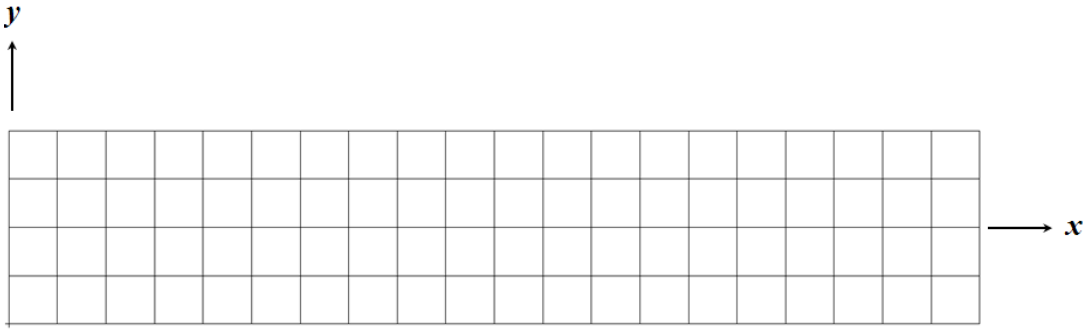

Figure 4-3 Background mesh for cantilever beam problem

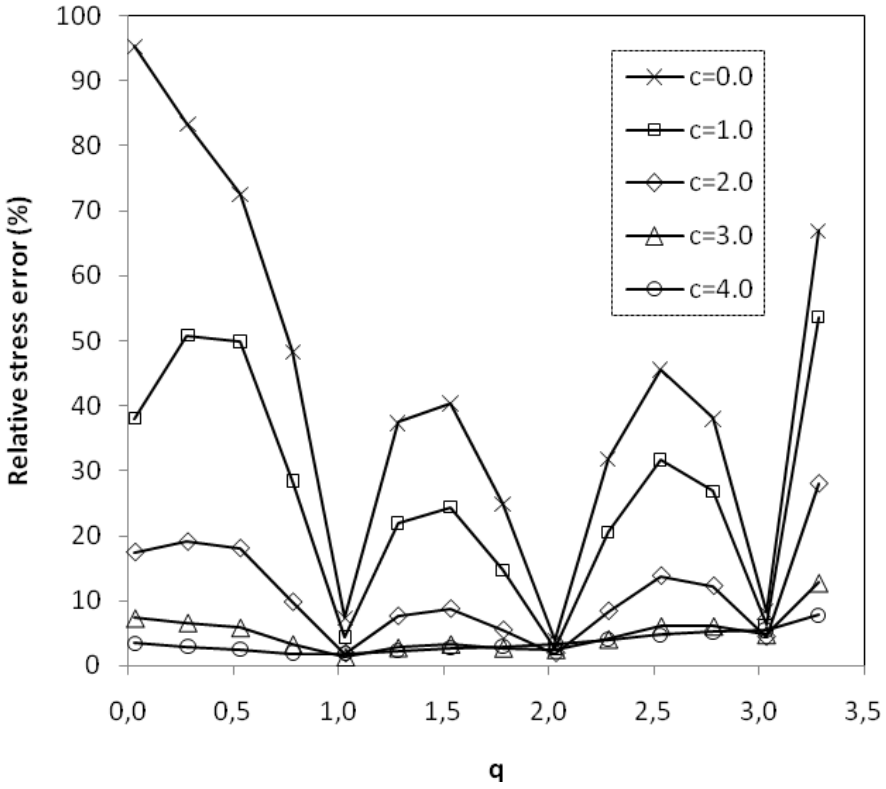

Figure 4-4 Effect of parameter q for different values of c on the relative stress error in cantilever beam problem

First, the problem is solved with given parameters above for different values of shape parameters c and q without polynomial terms added in the interpolation. Figure 4-4 shows the variation of the relative percentage stress error with respect to q for different values of c. It is seen that error makes minimum around integer values of parameter q but not exactly at integer values for different values of parameter c. This is the observation made by Wang and Liu [31] and the optimal value recommended for parameter q is 1.03. It also observed from Figure 4-4 that the sensitivity of error decreases with respect to q when parameter c increases.

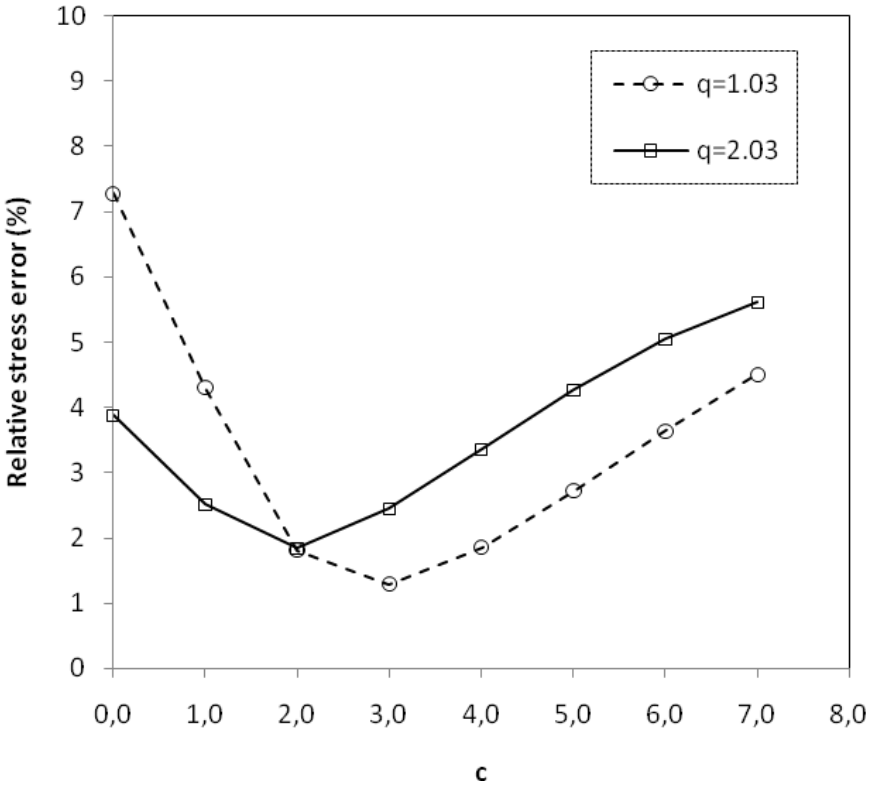

Figure 4-5 Effect of parameter c for q=1.03 and 2.03 on the relative stress error in cantilever beam problem

Following the observations from Figure 4-4, values of parameter q is fixed to 1.03 and 2.03 and the effect of parameter c on the relative percentage stress error is plotted as shown in Figure 4-5. Considering the results for both values of parameter q, the minimum error is obtained at c=3.0 for q=1.03. This is in the range found for c (3.0-7.0) by Liu and Gu [32].

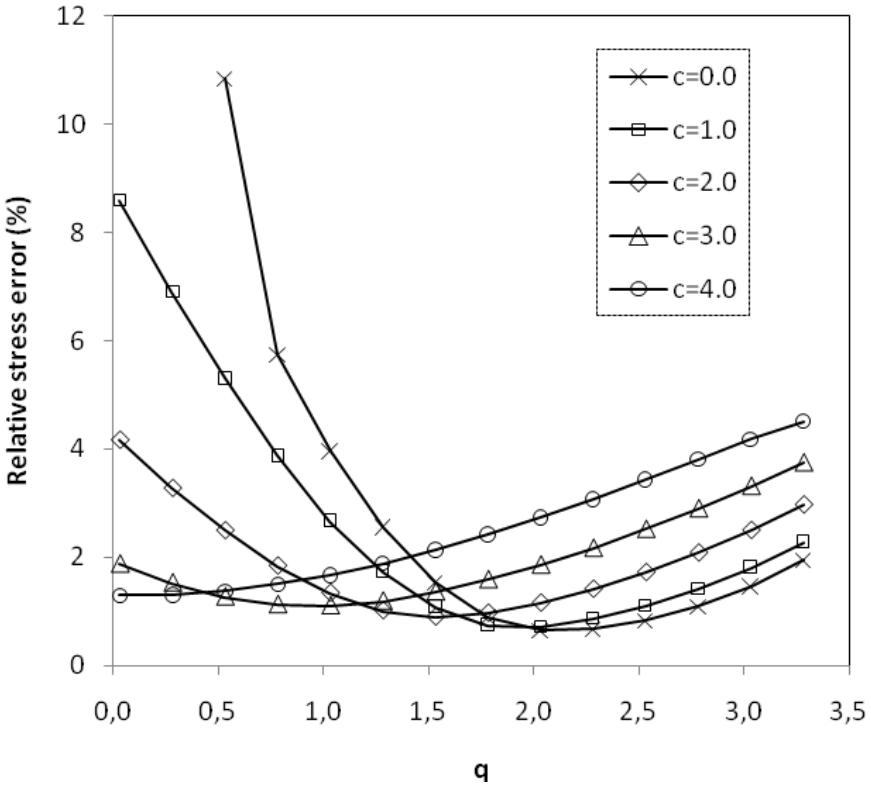

Figure 4-6 Effect of parameter q for different values of c with polynomial terms on the relative stress error in cantilever beam problem

Next, the problem is solved for different values of shape parameters c and q with polynomial terms added in the interpolation to see whether optimal values of parameters c and q changes or not. Figure 4-6 shows effect of parameter q on the relative percentage stress error for different values of c with polynomial terms added. Results show that the addition of polynomial terms decreases the error considerably. This is the observation made by Wang and Liu [31]. It is also observed that the addition of polynomial terms decreases the sensitivity of the error with respect to variations in both parameters c and q and in contrast to the case without polynomial terms, optimal values for parameter q varies for different values of parameter c. As the parameter c increases the optimal value of parameter q decreases and the minimum value of error increases.

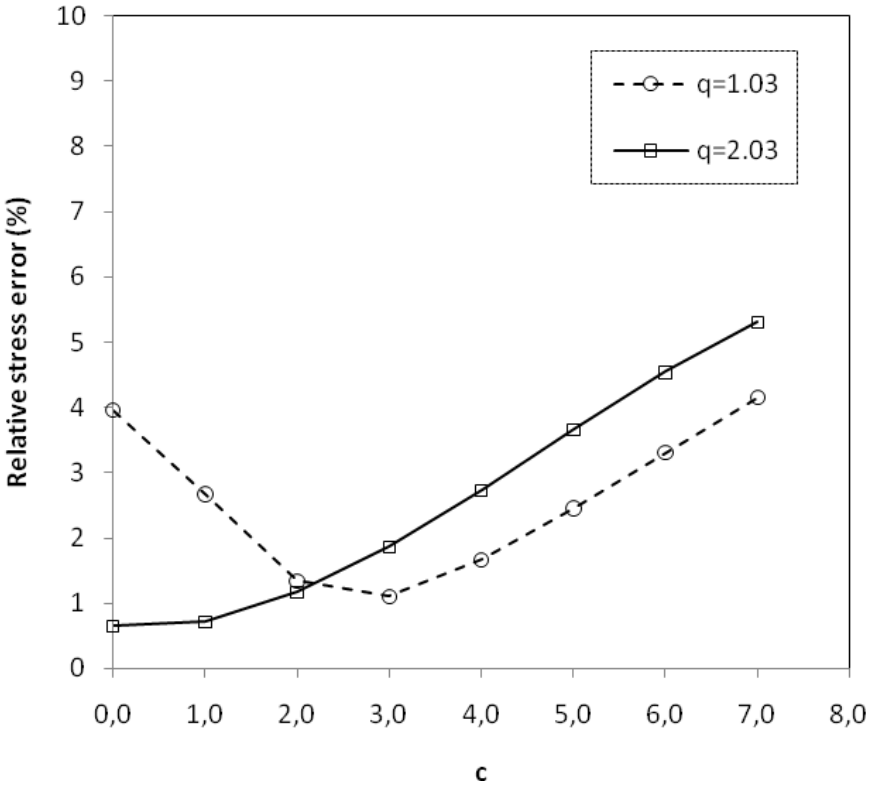

Figure 4-7 Effect of parameter c for q=1.03 and 2.03 with polynomial terms on the relative stress error in cantilever beam problem

Values of parameter q is fixed to 1.03 and 2.03 and the effect of parameter c on the relative percentage stress error with polynomial terms is plotted as shown in Figure 4-7. Variation of the error with respect to parameter c for q=1.03 is similar to the case with polynomial terms and c=3.0 again gives the minimum error. However, considering the results for both values of parameter q, the minimum error is obtained at c=0.0 for q=2.03.

Figure 4-8 shows the deflection v at y=0 for shape parameter q=2.03 and c=0.0 with polynomial terms. Figure 4-9, Figure 4-10 and Figure 4-11 show distribution of σ_x, σ_y and τ_{xy} respectively at $x=l/2$ for shape parameter q=2.03 and c=0.0 with polynomial terms.

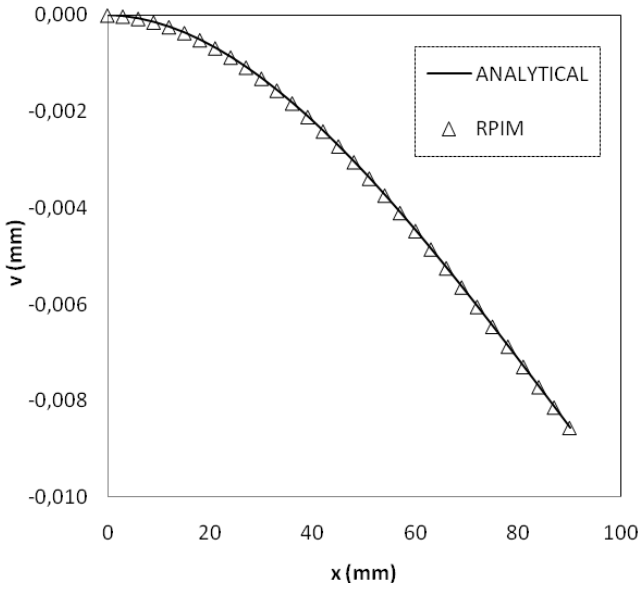

Figure 4-8 The deflection v at y=0 for shape parameter q=2.03 and c=0.0 with polynomial terms in cantilever beam problem

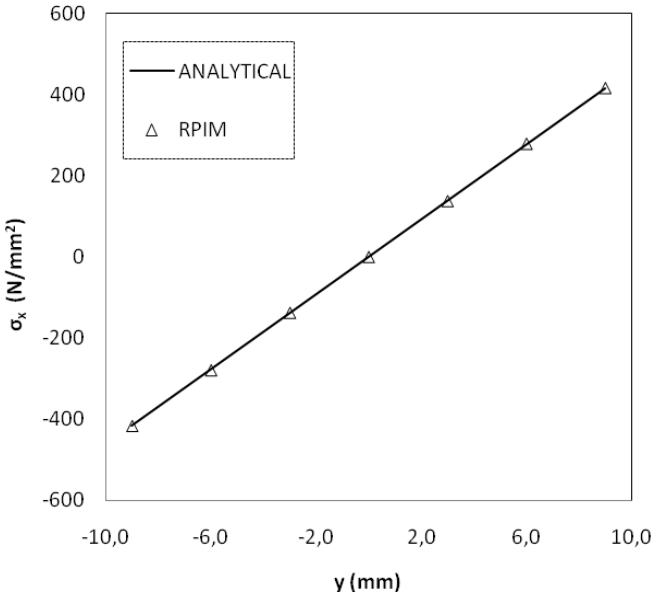

Figure 4-9 Distribution of σ_x at x=l/2 for shape parameter q=2.03 and c=0.0 with polynomial terms in cantilever beam problem

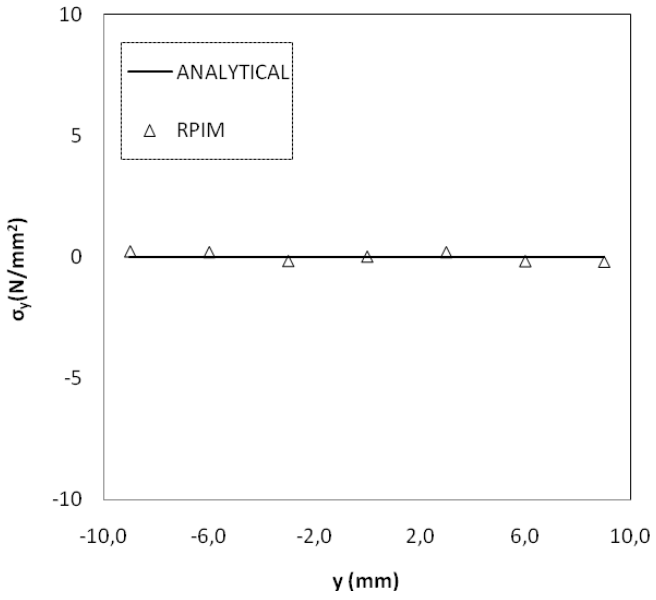

Figure 4-10 Distribution of σ_y at $x=l/2$ for shape parameter q=2.03 and c=0.0 with polynomial terms in cantilever beam problem

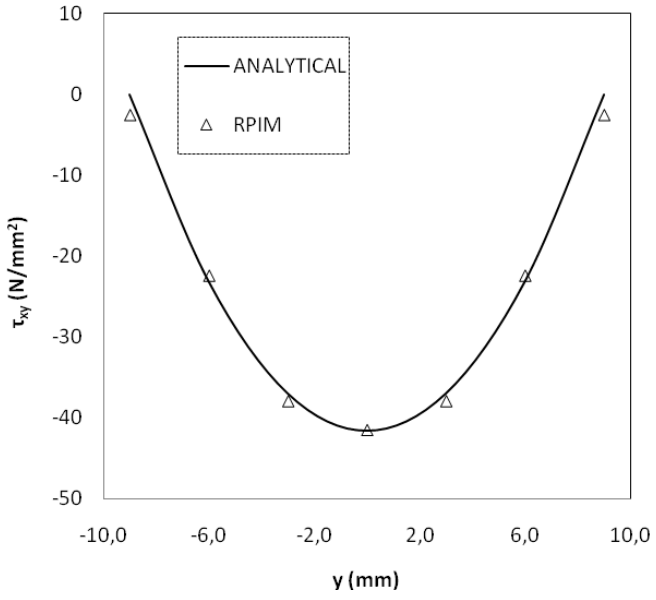

Figure 4-11 Distribution of τ_{xy} at $x=l/2$ for shape parameter q=2.03 and c=0.0 with polynomial terms in cantilever beam problem.

4.2 Infinite Plate with Circular Hole Under Uniform Far-Field Load

An infinite plate with circular hole subjected to uniform far-field load in *x* direction is shown in Figure 4-12.

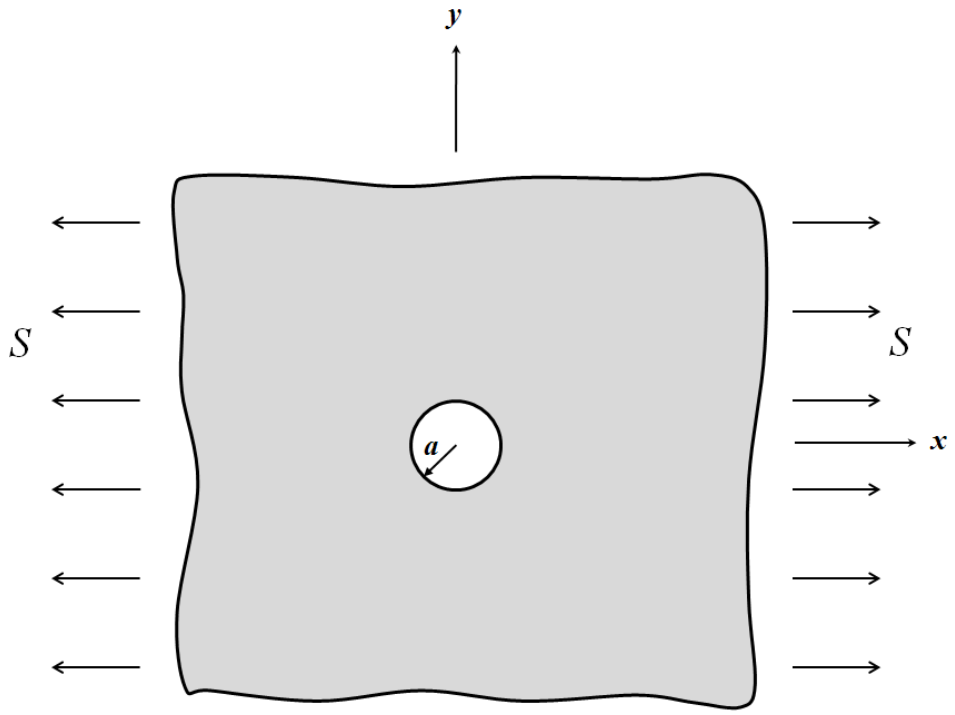

Figure 4-12 Infinite plate with circular hole under uniform far-field load

Analytical solution for this problem is given as follows [30],

The normal stress component in *x* direction is

$$\sigma_x = S\left\{1-\frac{a^2}{r}\left[\frac{3}{2}\cos(2\theta)+\cos(4\theta)\right]+\frac{3a^4}{2r^4}\cos(4\theta)\right\} \tag{4.10}$$

The normal stress component in y direction is

$$\sigma_y = -S\left\{\frac{a^2}{r}\left[\frac{1}{2}\cos(2\theta) - \cos(4\theta)\right] + \frac{3a^4}{2r^4}\cos(4\theta)\right\} \tag{4.11}$$

where (r,θ) are the polar coordinates and θ is measured from the positive x axis counterclockwise.

The shear stress is

$$\tau_{xy} = -S\left\{\frac{a^2}{r}\left[\frac{1}{2}\sin(2\theta) + \sin(4\theta)\right] - \frac{3a^4}{2r^4}\sin(4\theta)\right\} \tag{4.12}$$

The displacement components are

$$u_r = \frac{S}{4G}\left\{r\left[\frac{\kappa - 1}{2} + \cos(2\theta)\right] + \frac{a^2}{r}\left[1 + (1+\kappa)\cos(2\theta)\right] - \frac{a^4}{r^3}\cos(2\theta)\right\} \tag{4.13}$$

$$u_\theta = \frac{S}{4G}\left[(1-\kappa)\frac{a^2}{r} - r - \frac{a^4}{r^3}\right]\sin(2\theta) \tag{4.14}$$

where G is shear modulus given by

$$G = \frac{E}{2(1+\nu)} \tag{4.15}$$

and κ is Kolosov constant given by

$$\kappa = \frac{3-\nu}{1+\nu} \tag{4.16}$$

The solution of a square finite plate with an edge length ten times greater than radius of the hole is very close to solution of the infinite plate. Considering the symmetry of the problem also, only one quarter of the plate is modelled as shown in Figure 4-13.

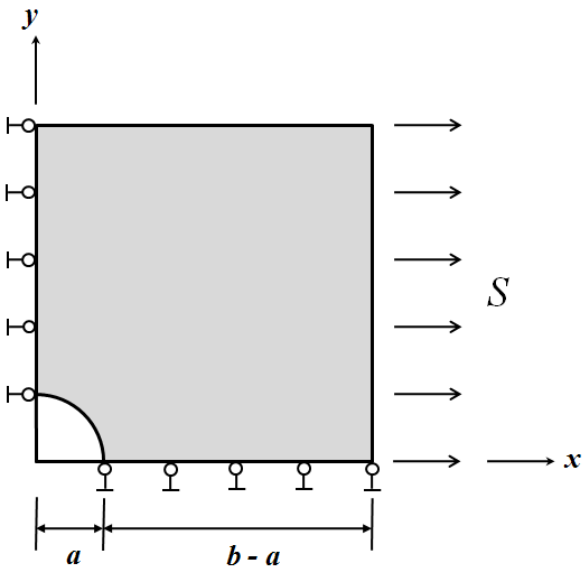

Figure 4-13 Upper right quarter model of square finite plate with circular hole under uniform far-field load

Parameters for this problem are given in Table 4-2.

Table 4-2 Parameters for the problem of square finite plate with circular hole under uniform far-field load

Parameter	Value
Load, S	1.0 N/m
Young's modulus, E	1000 N/m^2
Poisson's ratio, υ	0.3
a	1.0 m
b	5.0 m

The problem is solved for plane stress case. The domain of upper right quarter of square finite plate with circular hole is modelled using 293 distributed field nodes as shown in Figure 4-14. A background mesh of 99 quadrilateral cells as shown in Figure 4-15 are used for numerical integration. 4*4 Gauss points are used in each cell. Circular support domains are defined and fixed number (30) of nodes is used in support domain of each Gauss point for displacement interpolation.

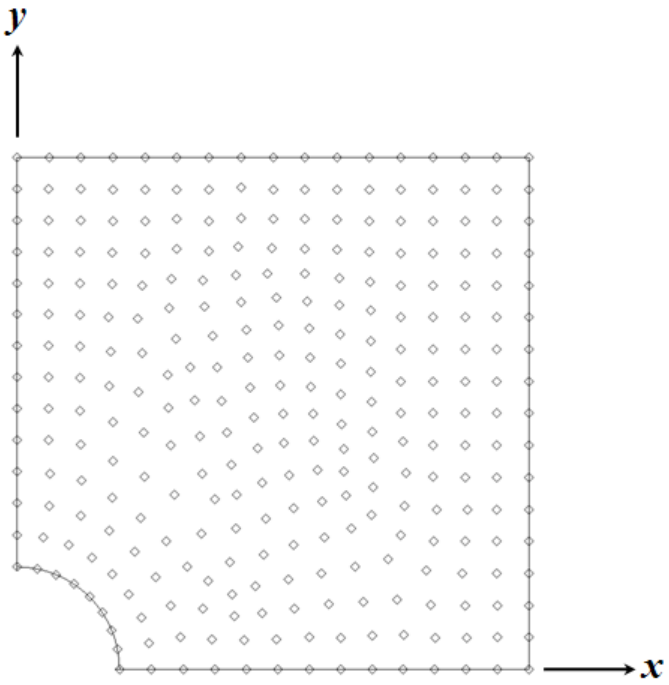

Figure 4-14 Node distribution for infinite plate with circular hole problem

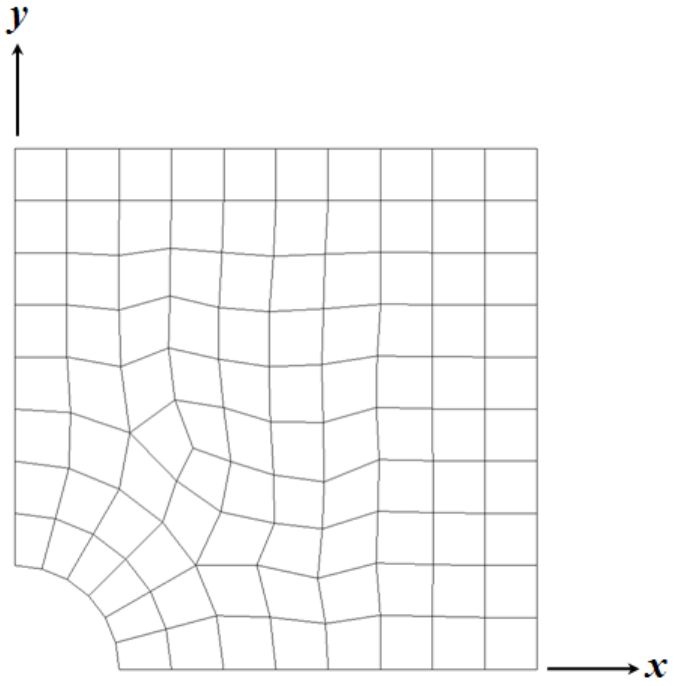

Figure 4-15 Background mesh for infinite plate with circular hole problem

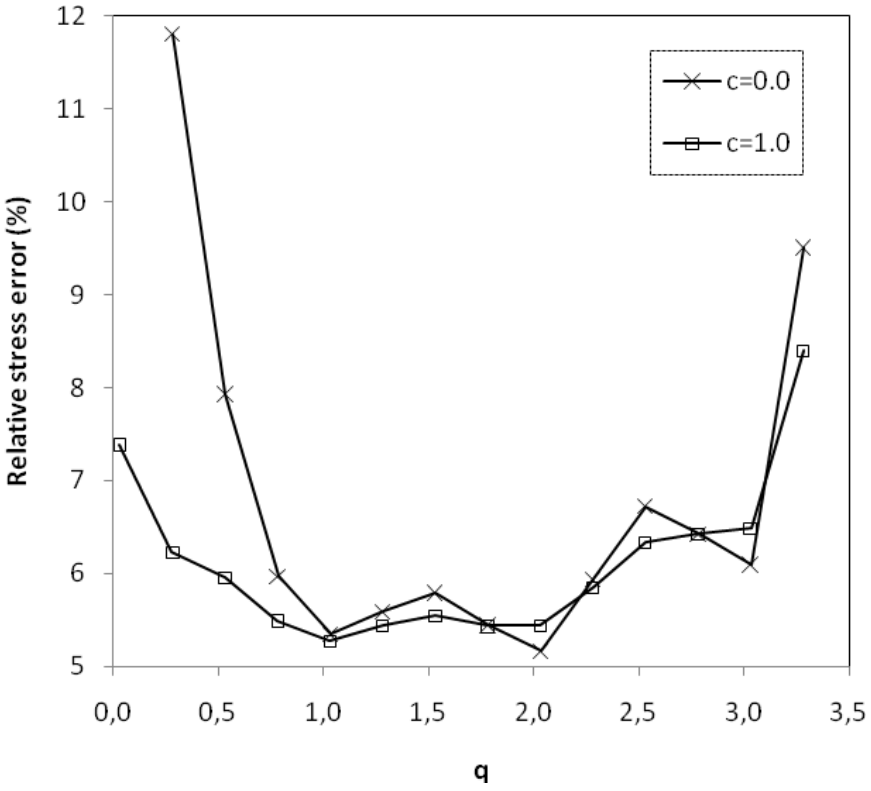

Figure 4-16 Effect of parameter q for different values of c on the relative stress error in infinite plate with circular hole problem

First, the problem is solved with given parameters above for different values of shape parameters c and q without polynomial terms added in the interpolation. Figure 4-16 shows the effect of parameter q on the relative percentage stress error for different values of c. Similar to the cantilever beam problem, it is observed that error makes minimum around integer values (1 and 2) of parameter q for different values of parameter c. But this time, variation in error is less sensitive to parameter q.

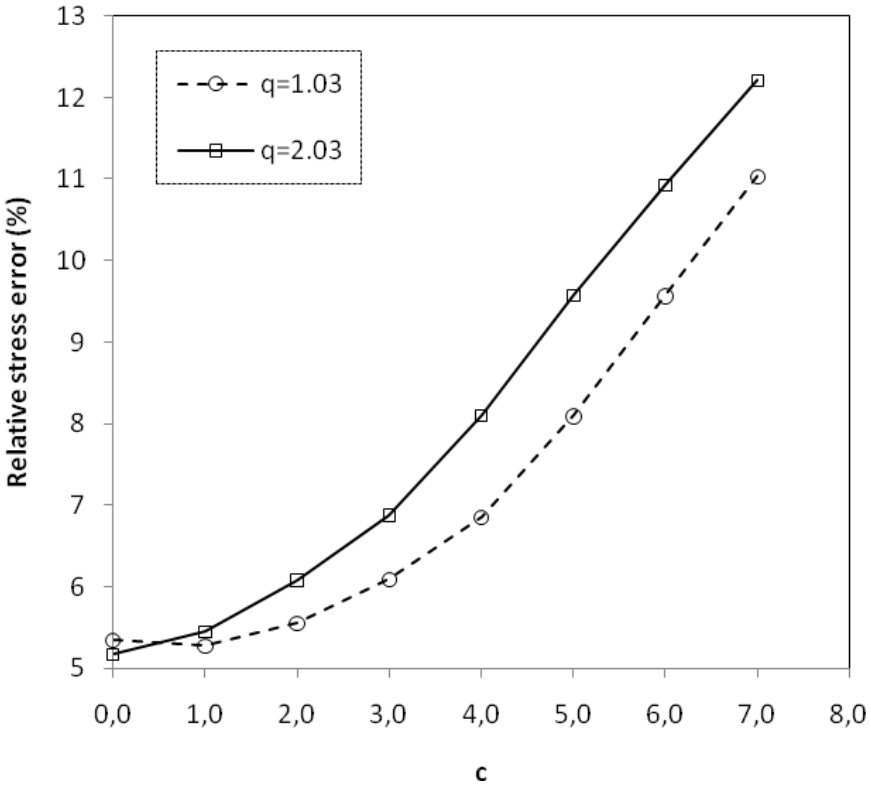

Figure 4-17 Effect of parameter *c* for *q*=1.03 and 2.03 on the relative stress error in infinite plate with circular hole problem

Again values of parameter *q* is fixed to 1.03 and 2.03 and the effect of parameter *c* in the range of 0.0 - 7.0 on the relative percentage stress error is plotted as shown in Figure 4-17. It seen that optimal values of parameter *c* change when compared to the cantilever beam problem. For both values of parameter *q*, optimal value of *c* is close to 0.0. This is out of the range found for *c* (3.0-7.0) by Liu and Gu [32].

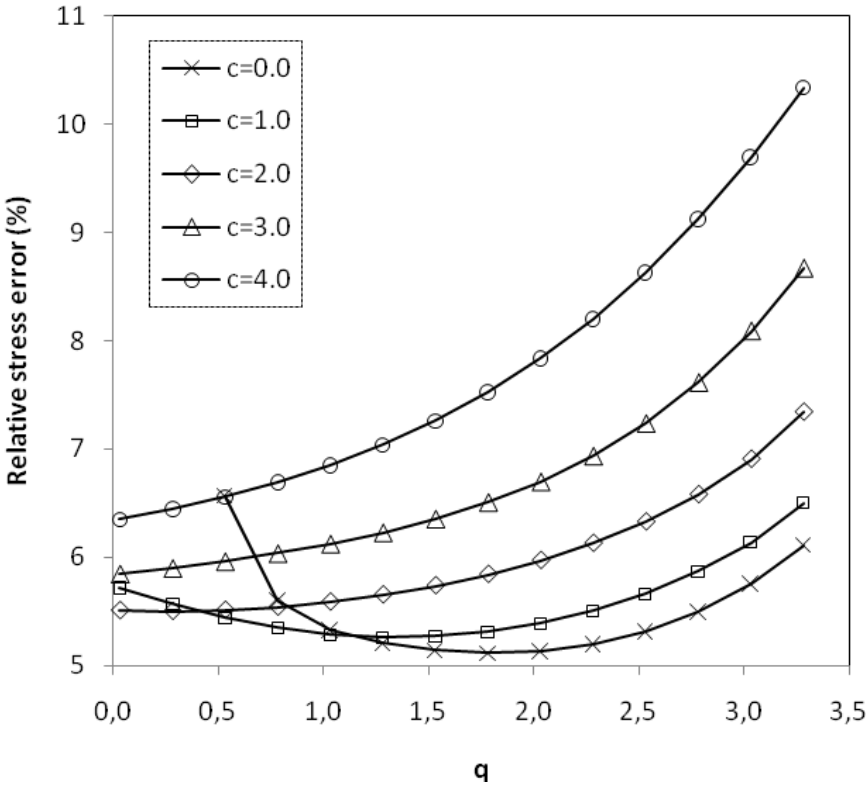

Figure 4-18 Effect of parameter q for different values of c with polynomial terms on the relative stress error in infinite plate with circular hole problem

Next, the problem is solved for different values of shape parameters c and q with polynomial terms added in the interpolation to see whether optimal values of parameters c and q changes or not. Figure 4-18 shows effect of parameter q on the relative percentage stress error for different values of c with polynomial terms added. The sensitivity of the error with respect to variations in both parameters c and q decreases with the addition of polynomial terms. Similar observations can be made for the optimal values of parameters as the cantilever beam problem. As the parameter c increases the optimal value of parameter q decreases and the minimum value of error increases.

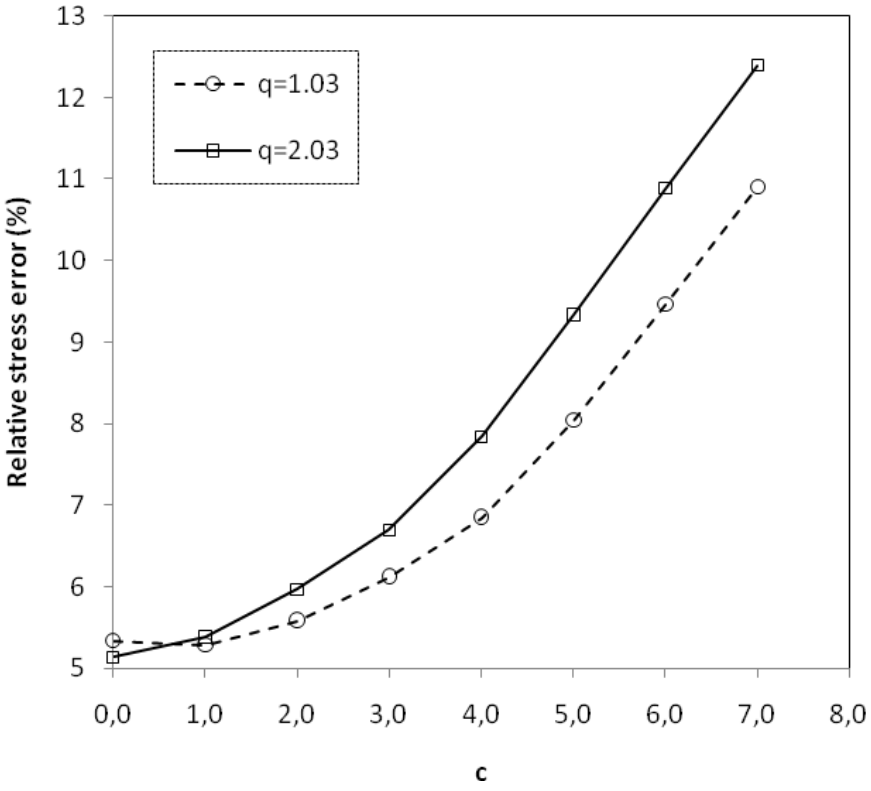

Figure 4-19 Effect of parameter c for q=1.03 and 2.03 with polynomial terms on the relative stress error in infinite plate with circular hole problem

Figure 4-19 shows the effect of parameter c for q=1.03 and 2.03 with polynomial terms on the relative percentage stress error. The minimum error is obtained at c=0.0 for q=2.03. It is also observed that optimal values of parameter c do not change with the addition of polynomial terms. This is different than the observation in cantilever beam problem where addition of polynomial terms change the optimal value of parameter c for q=2.03.

4.3 Thick-Walled Hollow Cylinder Under Uniform Internal Pressure

Another plane elasticity problem considered is a hollow thick-walled cylinder subjected to a uniform internal pressure p shown in Figure 4-20.

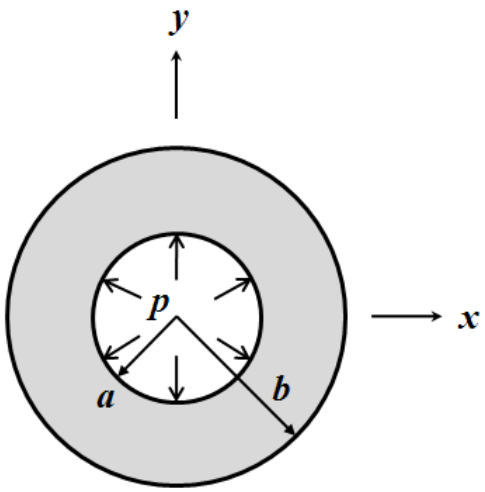

Figure 4-20 Hollow thick-walled cylinder subjected to a uniform internal pressure

Analytical solution for this problem is given as follows[30]

The normal stress component in radial direction is

$$\sigma_r = \frac{a^2 p}{b^2 - a^2}\left(1 - \frac{b^2}{r^2}\right) \tag{4.17}$$

The normal stress component in tangential direction is

$$\sigma_\theta = \frac{a^2 p}{b^2 - a^2}\left(1 + \frac{b^2}{r^2}\right) \tag{4.18}$$

The displacement component in radial direction is

$$u_r = \frac{a^2 pr}{E\left(b^2 - a^2\right)}\left[\left(1-\nu\right) + \left(1+\nu\right)\frac{b^2}{r^2}\right] \tag{4.19}$$

Parameters for this problem are chosen as in Table 4-3.

Table 4-3 Parameters for the problem of hollow thick-walled cylinder subjected to a uniform internal pressure

Parameter	Value
Load, *P*	100 N/mm
Young's modulus, *E*	12000 N/mm^2
Poisson's ratio, υ	0.3
Inner radius, *a*	10.0 mm
Outer radius, *b*	25.0 mm

Considering the symmetry of the problem, only one quarter of the is modelled as shown in Figure 4-21.

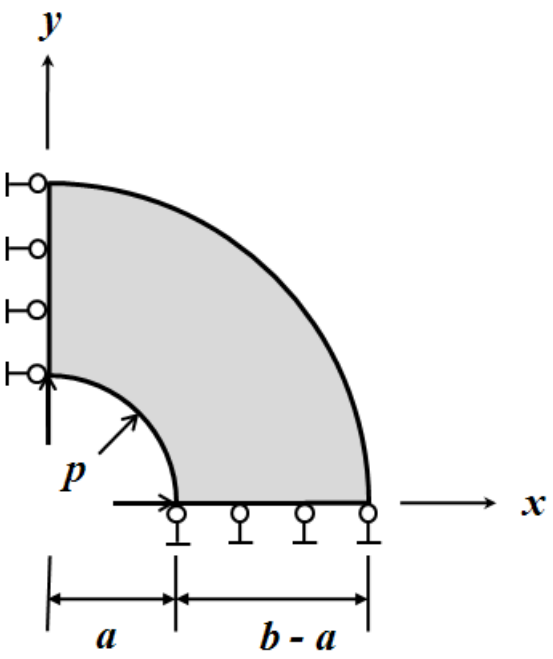

Figure 4-21 Upper right quarter model of hollow thick-walled cylinder subjected to a uniform internal pressure

The problem is solved for plane strain case. The domain of upper right quarter of hollow thick-walled cylinder is modelled using 189 distributed field nodes as shown in Figure 4-22. A background mesh of 78 quadrilateral cells as shown in Figure 4-23 are used for numerical integration. 4*4 Gauss points are used in each cell. Circular support domains are defined and fixed number (30) of nodes is used in support domain of each Gauss point for displacement interpolation.

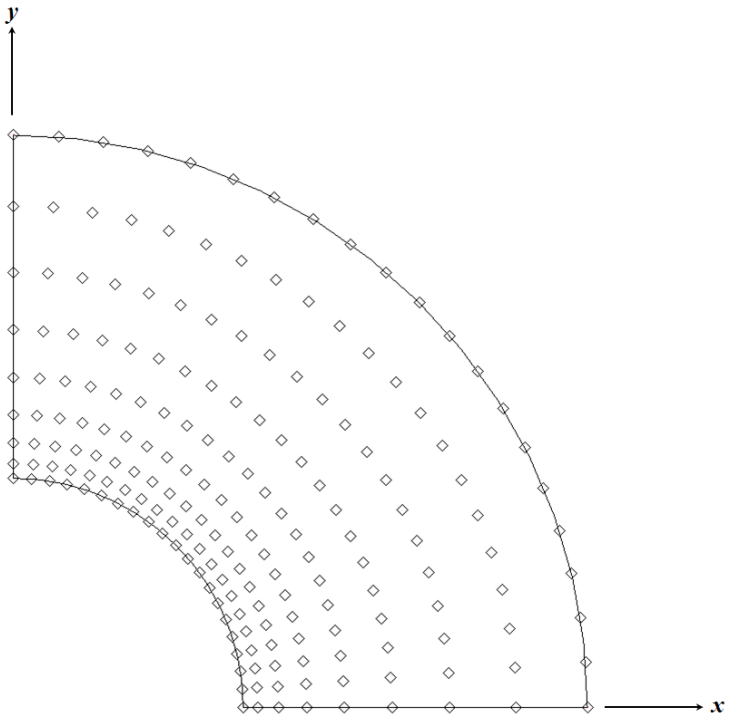

Figure 4-22 Node distribution for hollow thick-walled cylinder problem

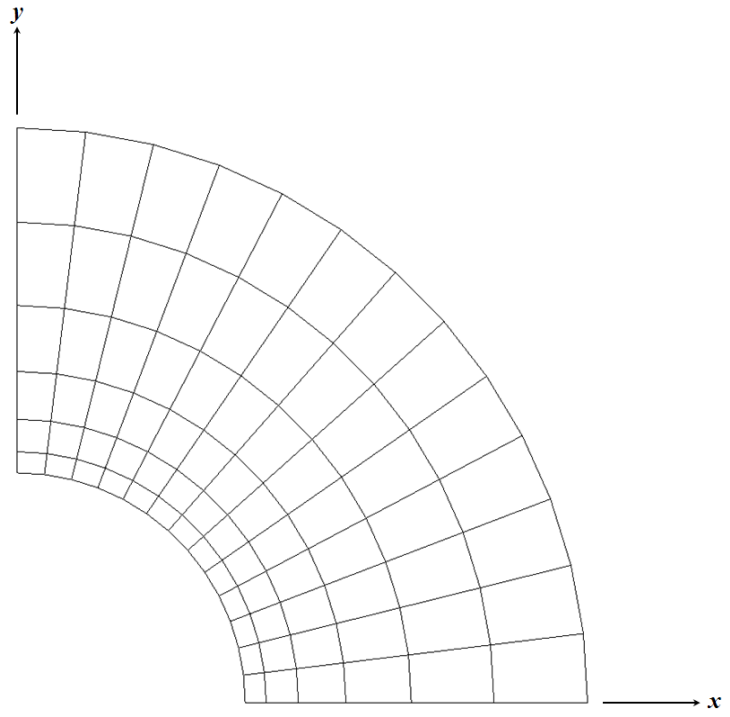

Figure 4-23 Background mesh for hollow thick-walled cylinder problem

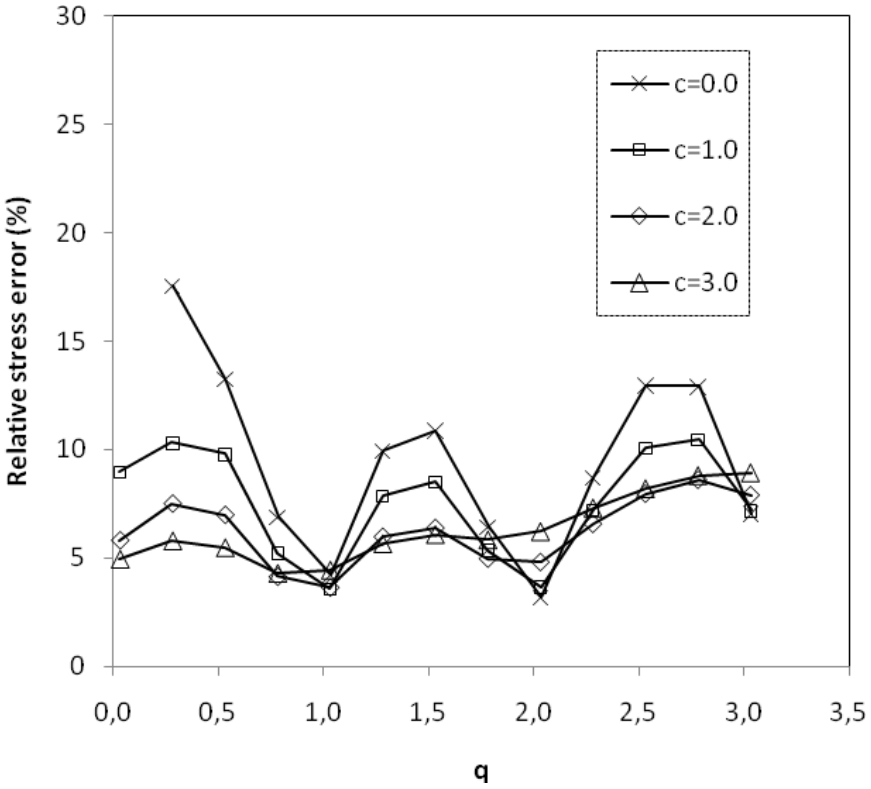

Figure 4-24 Effect of parameter *q* for different values of *c* on the relative stress error in hollow thick-walled cylinder problem

First, the problem is solved with given parameters above for different values of shape parameters *c* and *q* without polynomial terms added in the interpolation. Figure 4-24 shows the variation of the relative percentage stress error with respect to *q* for different values of *c*. Similar to results of the previous problems, error makes minimum around integer values of parameter *q* for different values of parameter *c*. As observed in the cantilever beam problem, the sensitivity of error decreases with respect to *q* when parameter c increases.

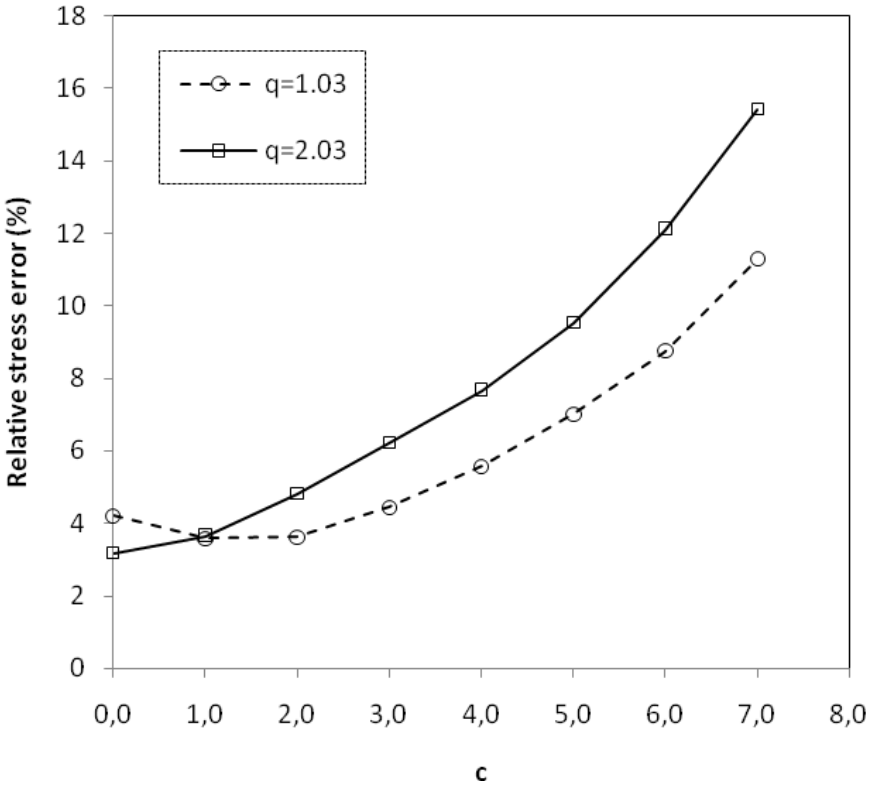

Figure 4-25 Effect of parameter *c* for *q*=1.03 and 2.03 on the relative stress error in hollow thick-walled cylinder problem

The effect of parameter *c* on the relative percentage stress error for *q*=1.03 and 2.03 is plotted as shown in Figure 4-25. Results are similar to those of infinite plate with circular hole problem. For both values of parameter *q*, optimal value of *c* is close to 0.0.

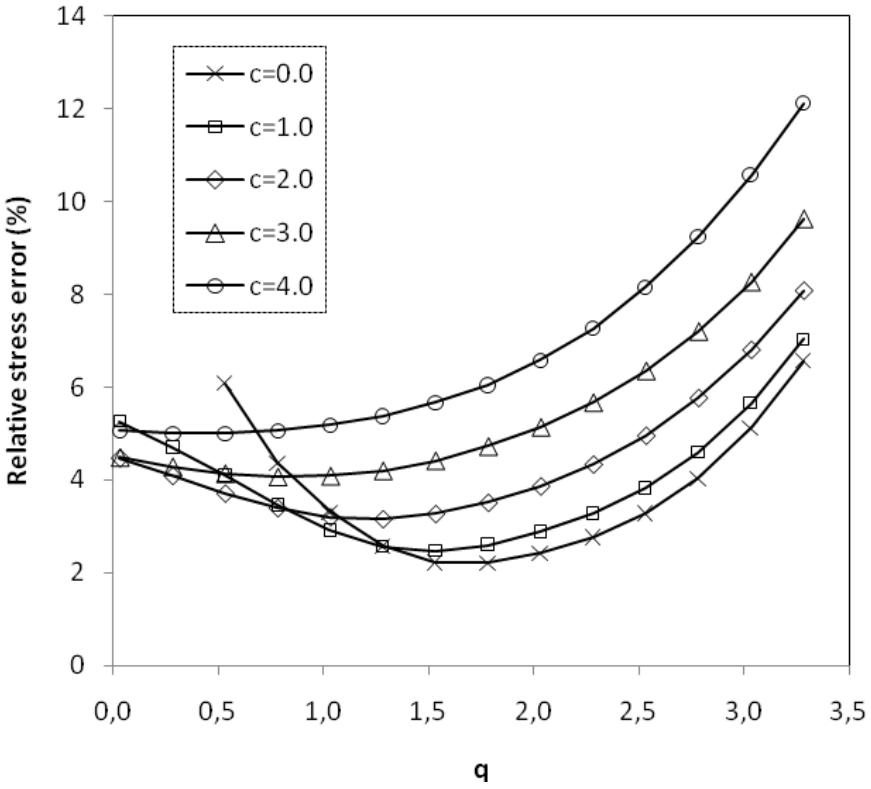

Figure 4-26 Effect of parameter *q* for different values of *c* with polynomial terms on the relative stress error in hollow thick-walled cylinder problem

Next, the problem is solved for different values of shape parameters *c* and *q* with polynomial terms added in the interpolation to see whether optimal values of parameters *c* and *q* changes or not. Figure 4-26 shows effect of parameter *q* on the relative percentage stress error for different values of *c* with polynomial terms added. Similar observations can be made as previous examples for the sensitivity and the decrease in error and the variation of optimal shape parameters with the addition of polynomial terms.

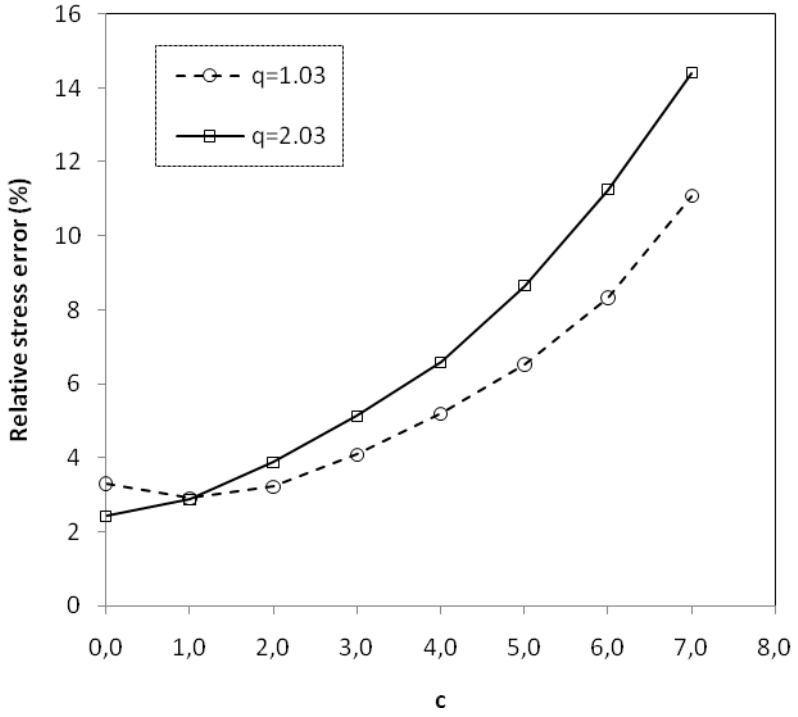

Figure 4-27 Effect of parameter c for q=1.03 and 2.03 with polynomial terms on the relative stress error in hollow thick-walled cylinder problem

Figure 4-27shows the effect of parameter c for q=1.03 and 2.03 with polynomial terms on the relative percentage stress error. Results are again similar to those of infinite plate with circular hole problem. The minimum error is obtained at c=0.0 for q=2.03 and the optimal values of parameter c do not change with the addition of polynomial terms.

Figure 4-28 and Figure 4-29 show distribution of u_r at θ=45^o and at r=10 respectively for shape parameter q=2.03 and c=0.0 with polynomial terms. Figure 4-30 shows distribution of σ_r at θ=45^o for shape parameter q=2.03 and c=0.0 with polynomial terms. Figure 4-31 shows distribution of σ_θ at θ=45^o for shape parameter q=2.03 and c=0.0 with polynomial terms.

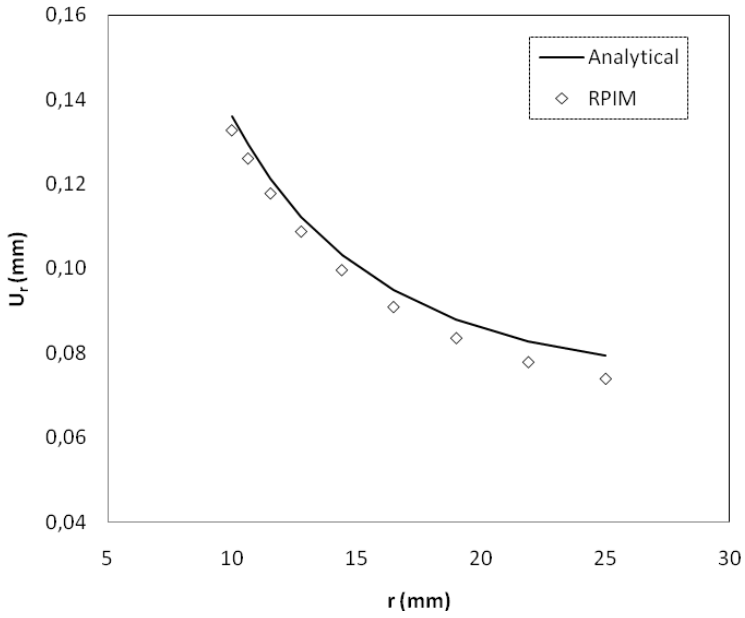

Figure 4-28 Distribution of u_r at θ=45^o for shape parameter q=2.03 and c=0.0 with polynomial terms in hollow thick-walled cylinder problem

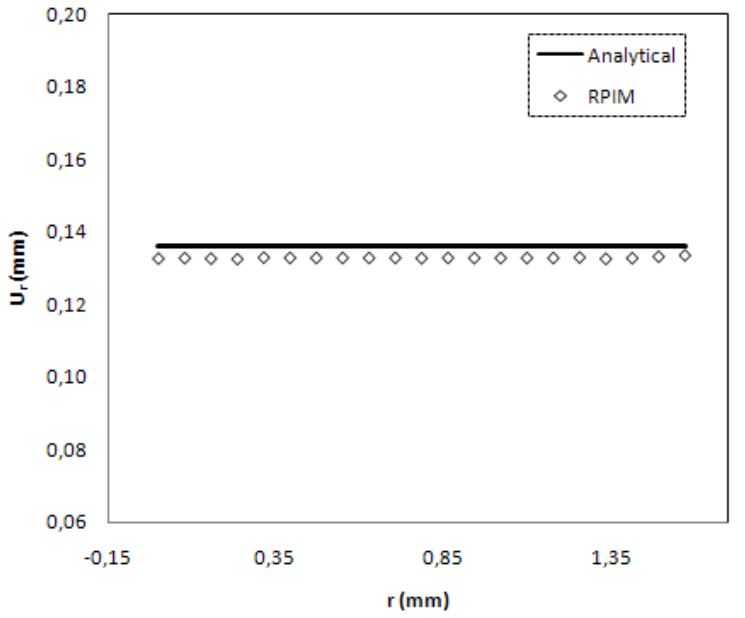

Figure 4-29 Distribution of u_r at r=10 for shape parameter q=2.03 and c=0.0 with polynomial terms in hollow thick-walled cylinder problem

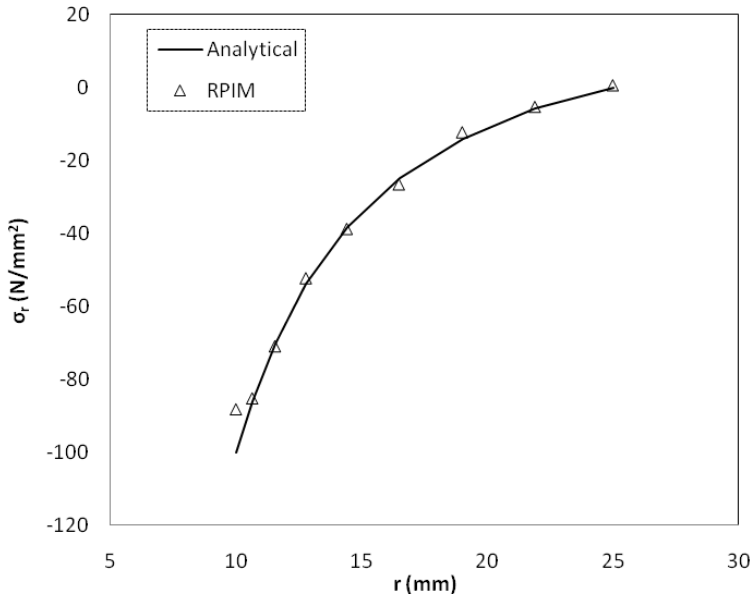

Figure 4-30 Distribution of σ_r at θ=45^o for shape parameter q=2.03 and c=0.0 with polynomial terms in hollow thick-walled cylinder problem

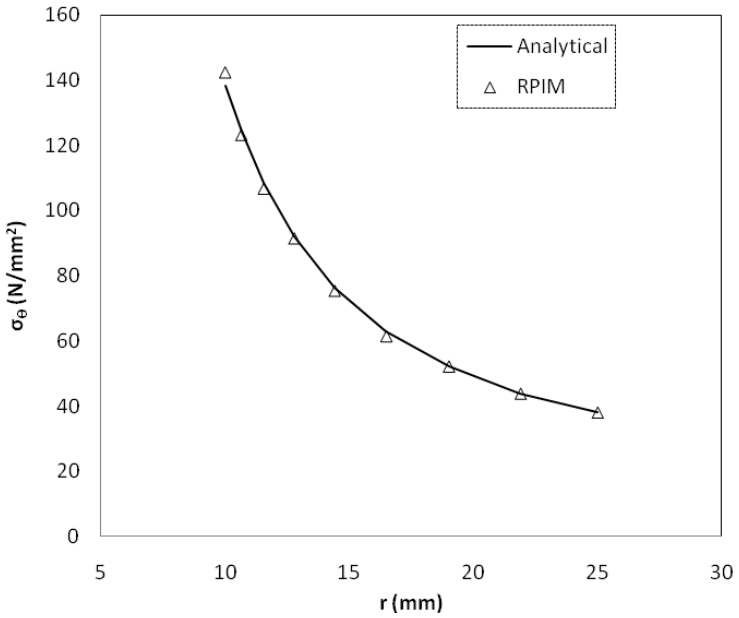

Figure 4-31 Distribution of σ_θ at θ=45^o for shape parameter q=2.03 and c=0.0 with polynomial terms in hollow thick-walled cylinder problem

4.4 Curved Beam Loaded at The End

Finally, the problem of a curved beam having a narrow rectangular cross section of unit width with a circular axis constrained at the upper end and bent by a force P applied at the lower end in the radial direction as shown in Figure 4-32.

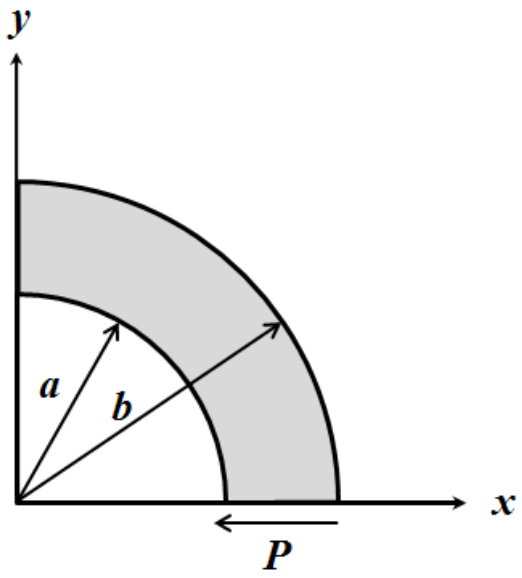

Figure 4-32 Curved beam loaded at the end

Analytical solution of the problem is given as follows [30].

The normal stress component in radial direction is

$$\sigma_r = \left(2Ar - \frac{2B}{r^3} + \frac{D}{r} \right) \sin(\theta) \tag{4.20}$$

The normal stress component in tangential direction is

$$\sigma_\theta = \left(6Ar + \frac{2B}{r^3} + \frac{D}{r}\right)\sin(\theta) \tag{4.21}$$

and the shear stress is

$$\tau_{r\theta} = -\left(2Ar - \frac{2B}{r^3} + \frac{D}{r}\right)\cos(\theta) \tag{4.22}$$

where (r, θ) are the polar coordinates and θ is measured from the positive x axis counterclockwise and the constants A, B, D and N are given as,

$$A = \frac{P}{2N} \tag{4.23}$$

$$B = -\frac{Pa^2b^2}{2N} \tag{4.24}$$

$$D = -\frac{P}{N}\left(a^2 + b^2\right) \tag{4.25}$$

where

$$N = a^2 - b^2 + \left(a^2 + b^2\right)\log\left(\frac{b}{a}\right) \tag{4.26}$$

The displacement components are

$$u_r = -\frac{2D}{E}\theta\cos(\theta) + \frac{\sin(\theta)}{E}\left[D(1-\upsilon)\log(r) + A(1-3\upsilon)r^2 + \frac{B(1+\upsilon)}{r^2}\right] + K\sin(\theta) + L\cos(\theta) \tag{4.27}$$

$$u_\theta = \frac{2D}{E}\theta\sin(\theta) - \frac{\cos(\theta)}{E}\left[A(5+\upsilon)r^2 + \frac{B(1+\upsilon)}{r} - D(1-\upsilon)\log(r) \right] + \frac{D(1+\upsilon)}{E}\cos(\theta) + K\cos(\theta) - L\sin(\theta) \tag{4.28}$$

where the constants K and L are given as,

$$K = -\frac{1}{E}\left[D(1-\upsilon)\log(r_0) + A(1-3\upsilon)r_0^{\,2} + \frac{B(1+\upsilon)}{r_0^{\,2}} \right] \quad \text{with} \quad r_0 = \frac{a+b}{2} \tag{4.29}$$

$$L = \frac{D\pi}{E} \tag{4.30}$$

Parameters for this problem are chosen as in Table 4-4.

Table 4-4 Parameters for the problem of curved beam loaded at the end

Parameter	Value
Load, P	1000 N/mm
Young's modulus, E	30000000 N/mm^2
Poisson's ratio, υ	0.3
Inner radius, a	18 mm
Outer radius, b	24 mm

The problem is solved for plane stress case. The domain of curved beam is modelled using 273 distributed field nodes as shown in Figure 4-33. A background mesh of 100 quadrilateral cells as shown in Figure 4-34 are used for numerical integration. 4*4 Gauss points are used in each cell. Circular support domains are defined and fixed number (30) of nodes is used in support domain of each Gauss point for displacement interpolation.

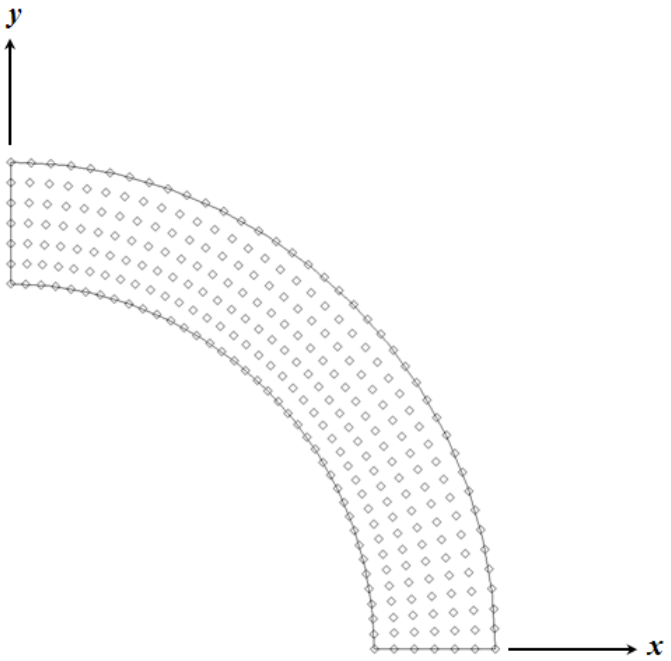

Figure 4-33 Node distribution for curved beam problem

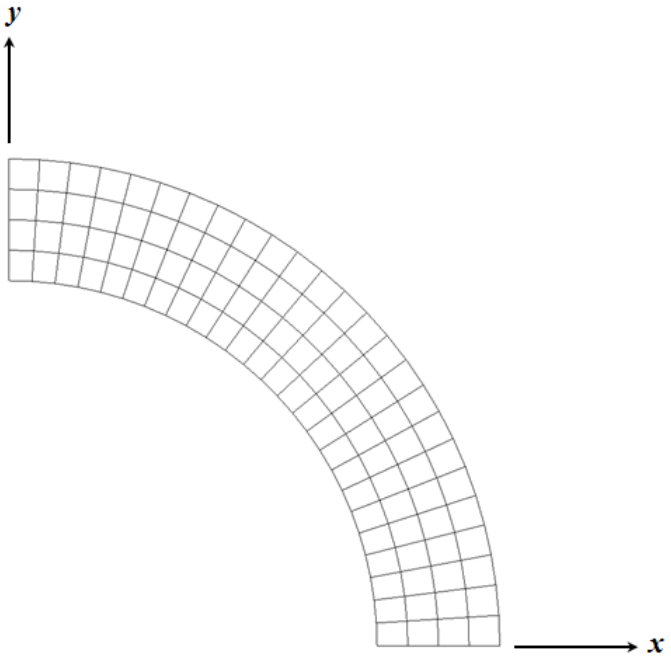

Figure 4-34 Background mesh for curved beam problem

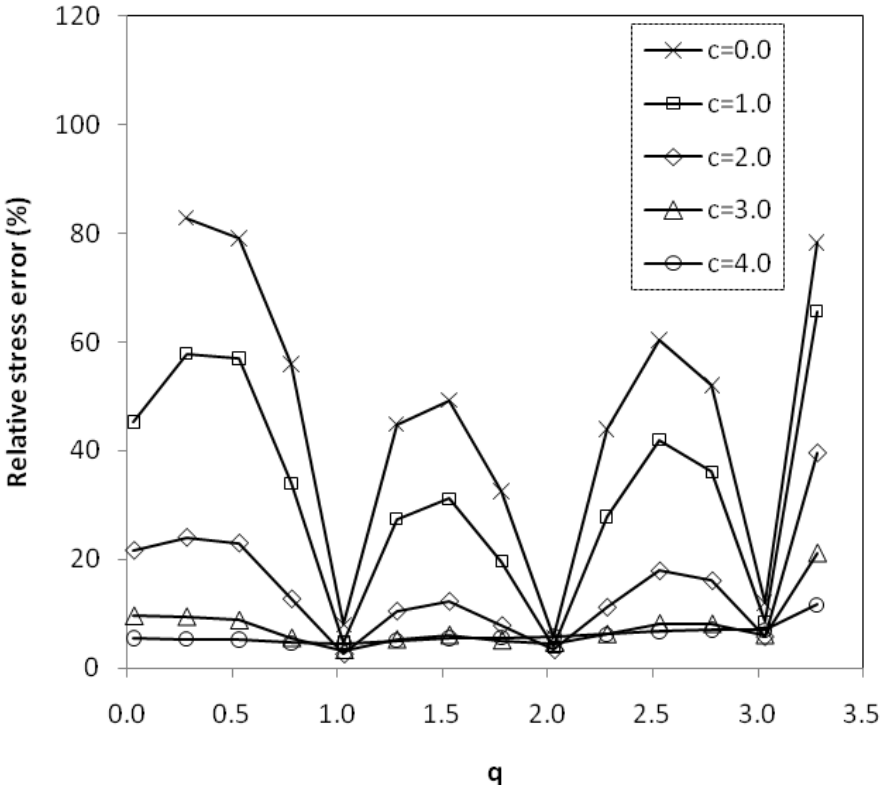

Figure 4-35 Effect of parameter q for different values of c on the relative stress error in curved beam problem

First, the problem is solved with given parameters above for different values of shape parameters c and q without polynomial terms added in the interpolation. Figure 4-35 shows the variation of the relative percentage stress error with respect to q for different values of c. Results are very similar to those of cantilever beam. So the same observations are valid here.

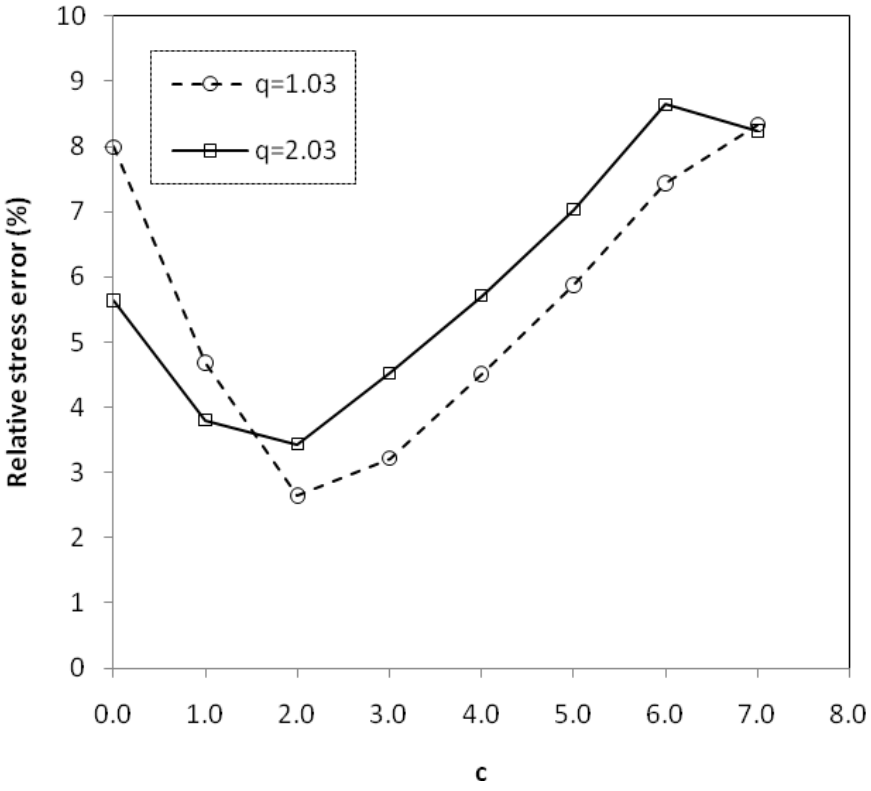

Figure 4-36 Effect of parameter *c* for *q*=1.03 and 2.03 on the relative stress error in curved beam problem

Values of parameter *q* is fixed to 1.03 and 2.03 and the effect of parameter *c* on the relative percentage stress error is plotted as shown in Figure 4-36. Considering the results for both values of parameter *q*, the minimum error is obtained at *c*=2.0 for *q*=1.03.

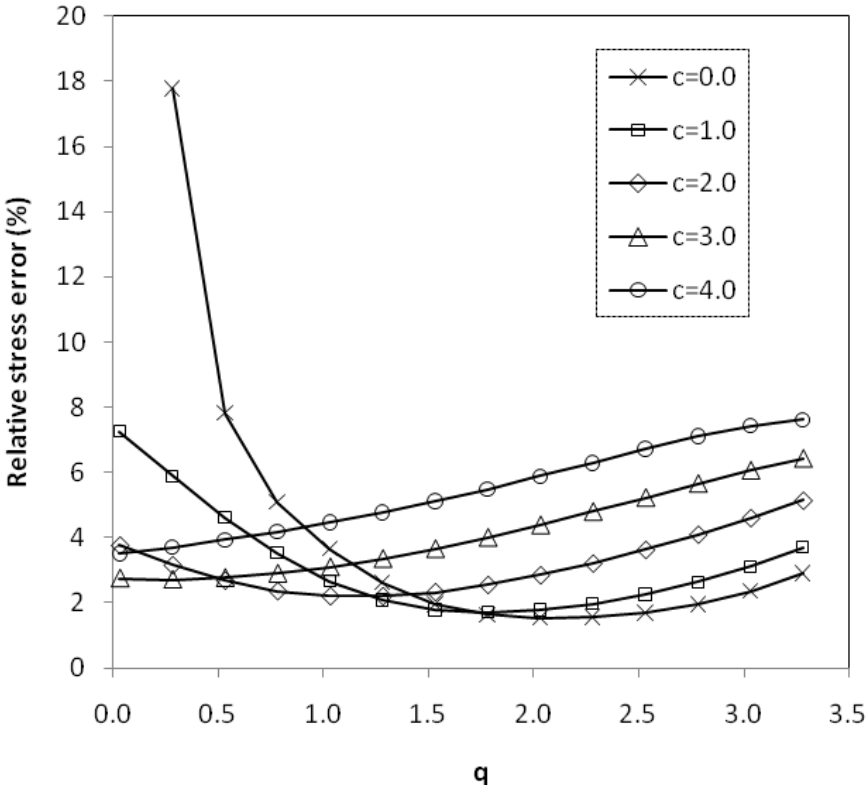

Figure 4-37 Effect of parameter *q* for different values of *c* with polynomial terms on the relative stress error in cantilever beam problem

Next, the problem is solved for different values of shape parameters c and q with polynomial terms added in the interpolation to see whether optimal values of parameters *c* and *q* changes or not. Figure 4-37 shows effect of parameter *q* on the relative percentage stress error for different values of *c* with polynomial terms added. Again results are very similar to those of cantilever beam problem with polynomial terms.

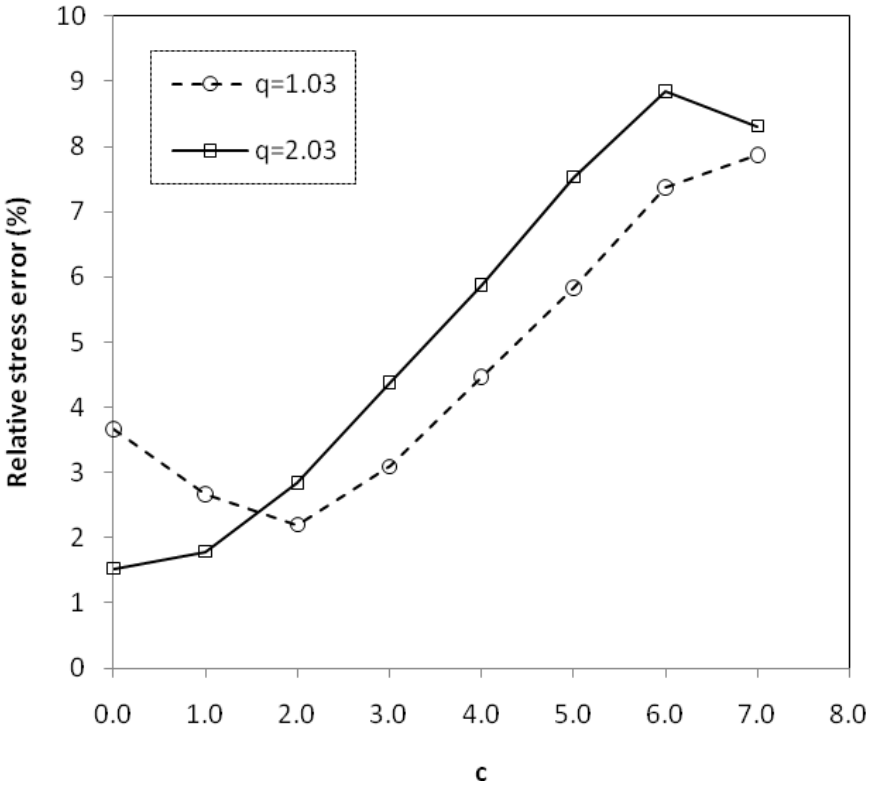

Figure 4-38 Effect of parameter c for q=1.03 and 2.03 with polynomial terms on the relative stress error in cantilever beam problem

Values of parameter q is fixed to 1.03 and 2.03 and the effect of parameter c on the relative percentage stress error with polynomial terms is plotted as shown in Figure 4-38. Variation of the error with to parameter c for q=1.03 is similar to the case with polynomial terms and c=2.0 again gives the minimum error. However, considering the results for both values of parameter q, the minimum error is obtained at c=0.0 for q=2.03.

Figure 4-39 shows the deflection u_r at r=21 mm for shape parameter q=2.03 and c=0.0 with polynomial terms in cantilever beam problem. Figure 4-40, Figure 4-41 and Figure 4-42 show distribution of σ_r, σ_θ and $\tau_{r\theta}$ respectively at $\theta = 45^0$ for shape parameter q=2.03 and c=0.0 with polynomial terms.

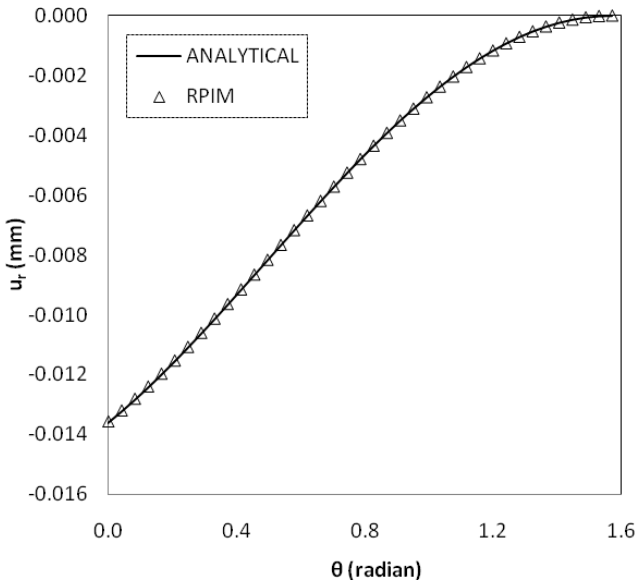

Figure 4-39 The deflection u_r at r=21 mm for shape parameter q=2.03 and c=0.0 with polynomial terms in cantilever beam problem.

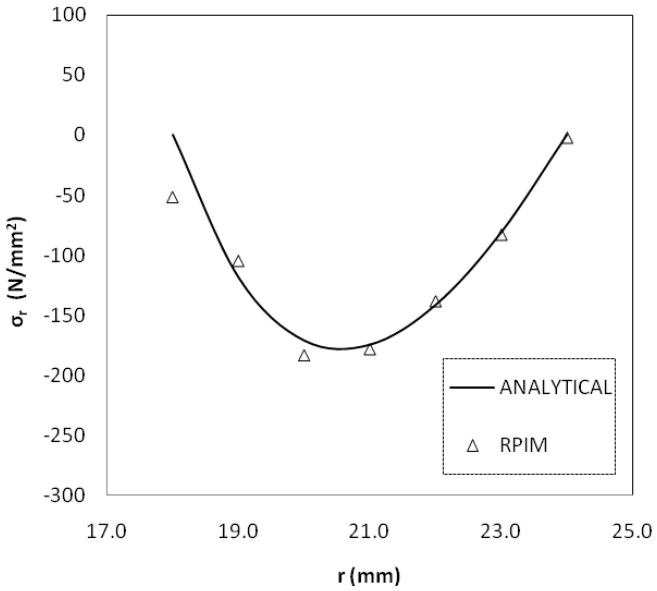

Figure 4-40 Distribution of σ_r at θ=45^0 for shape parameter q=2.03 and c=0.0 with polynomial terms in cantilever beam problem.

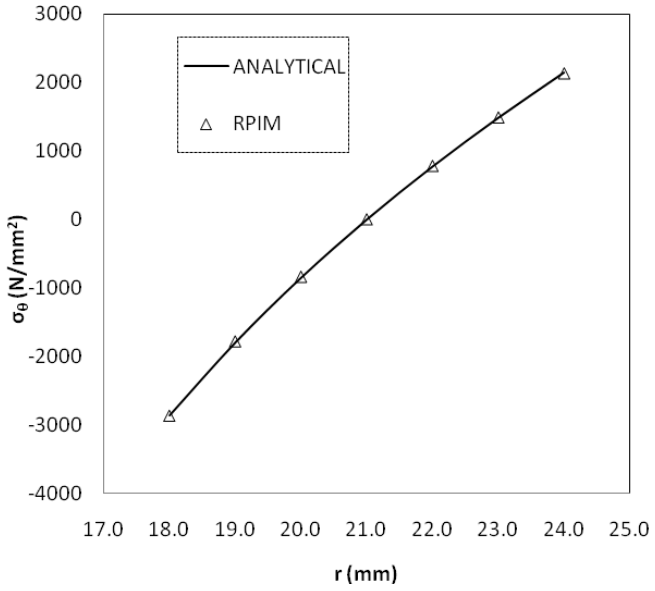

Figure 4-41 Distribution of σ_θ at θ=45^0 for shape parameter q=2.03 and c=0.0 with polynomial terms in cantilever beam problem.

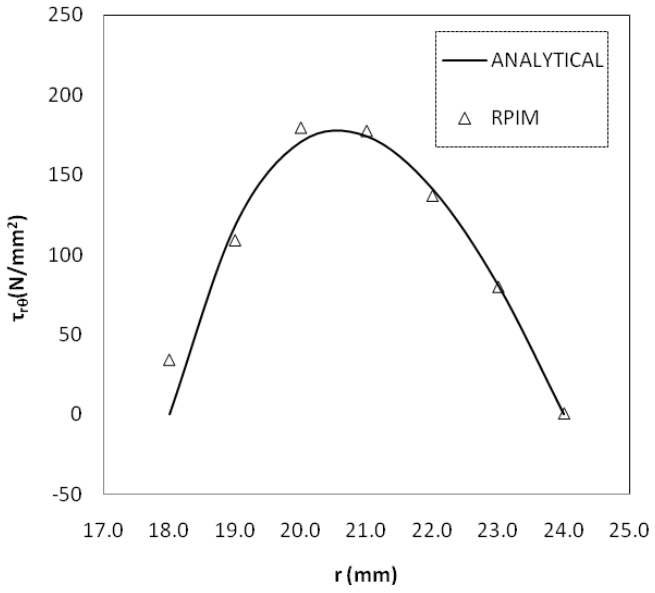

Figure 4-42 Distribution of $\tau_{r\theta}$ at θ=45^0 for shape parameter q=2.03 and c=0.0 with polynomial terms in cantilever beam problem.

CHAPTER 5

CONCLUSION

In this thesis, meshfree RPIM with MQ radial basis functions is implemented to analyze plane elasticity problems. A computer code implementing RPIM is developed with Fortran programming language and the effect of shape parameters on the accuracy of RPIM is studied through a stress error analysis to determine the optimal shape parameters.

Plane elasticity problems including cantilever beam loaded at the end, infinite plate with circular hole under uniform far-field load and thick-walled hollow cylinder under uniform internal pressure, whose analytical solutions are available in literature, are solved to illustrate the performance of RPIM.

A relative percentage stress error is defined for the error analysis. In each problem, effect of shape parameters of MQ radial basis functions is studied first without polynomial terms. Numerical results showed that shape parameter q around 1 and 2 gives accurate results. So, the effect of parameter c is studied with the value of parameter q is fixed to 1.03 to 2.03 and it is observed that the optimal value of parameter c differs for all studied problems. Second, the effect of parameters with polynomial terms added is studied. Numerical results showed that the optimal values of both parameters q and c are consistent for all studied problems. Parameter q around 2 and parameter c=0.0 gives the most accurate solution. It is also observed that the addition of polynomial terms reduces the relative stress error considerably for each case.

REFERENCES

[1] Lucy, L. B., "A Numerical Approach to the Testing of the Fission Hypothesis", The Astronomical Journal, 82, pp. 1013–1024, 1977.

[2] Gingold, R. A. and Monaghan, J. J., "Smoothed Particle Hydrodynamics: Theory and Application to Non-Spherical Stars", Monthly Notices of the Royal Astronomical Society, 181, pp. 375–389, 1977.

[3] Liszka, T. and Orkisz, J., "The finite difference methods at arbitrary irregular grids and its applications in applied mechanics" Computers and Structures, 11, pp. 83-95, 1980.

[4] Onate, E., Idelsohn, S., Zienkiewicz, O.C. and Taylor, R. L., "A finite point method in computational mechanic. Applications to convective transport and fluid flow" International Journal for Numerical Methods in Engineering, 39, pp. 3839 –3866, 1996.

[5] Onate, E., Idelsohn, S., Zienkiewicz, O. C., Taylor, R. L. and and Sacco, C., "A Stabilized Finite Point Method for Analysis of Fluid Mechanics Problems", Computer Methods in Applied Mechanics and Engineering, 139, pp. 315–346, 1996.

[6] Onate, E. and Idelsohn, S., "A Mesh Free Finite Point Method for Advective-Diffusive Transport and Fluid Flow Problems", Computational Mechanics, 21, pp. 283–292, 1998.

[7] Onate, E., Perazzo, F. and Miquel, J., "A Finite Point Method For Elasticity Problems", Computers and Structures, 79, pp. 2151–2163, 2001.

[8] Nayroles, B., Touzot, G. And Villon, P., “Generalizing the Finite Element Method: Diffuse Approximation and Diffuse Elements”, Computational Mechanics, 10, pp. 307–318, 1992.

[9] Lancaster, P. and Salkauskas, K., “Surfaces generated by moving least squares methods” Mathematics of Computation, 37, pp. 141–158, 1981.

[10] Belytschko, T., Lu, Y. Y. and Gu, L., “Element-Free Galerkin Methods”, International Journal for Numerical Methods in Engineering, 37, pp. 229–256, 1994.

[11] Liu, W. K., Jun, S. and Zhang, Y.F., “Reproducing Kernel Particle Methods”, International Journal for Numerical Methods in Fluids, 20, pp. 1081–1106, 1995.

[12] Aluru, N. R., “A point collocation method based on reproducing kernel approximations”, International Journal Numerical Methods in Engineering, 47, pp. 1083–1121, 2000.

[13] Duarte C.A. and Oden, J.T., “Hp clouds - a meshless method to solve boundary-value problems”, Computational Methods in Applied Mechanics and Engineering, 139:237–262, 1996

[14] Babuska, I. and Melenk, J. M. “The partition of unity finite element method: Basic theory and applications,” Comput. Methods Appl. Mech. Eng. 139, pp. 289–315, 1996.

[15] Mukherjee, Y. X. and Mukherjee, S. , “Boundary node method for potential Problems”, International Journal for Numerical Methods in Engineering vol. 40, pp. 797-815, 1997.

[16] Atluri, S. N. and Zhu, T., “A New Meshless Local Petrov-Galerkin (MLPG) Approach in Computational Mechanics”, Computational Mechanics, vol. 22, pp. 117–127, 1998.

[17] Liu, G. R. and Gu, Y. T., “A Point Interpolation Method in Proceeding”, 4th Asia–Pacific Conference on Computational Mechanics, Singapore, pp. 1009–1014, December 1999.

[18] Liu, G. R. and Gu, Y.T., "A Local Point Interpolation Method for Stress Analysis of Two-Dimensional Solids", Structural Engineering and Mechanics, 11, pp .221–236, 2001.

[19] Wang, J. G. and Liu, G. R., "Radial point interpolation method for elastoplastic problems in Proceeding" 1st Structural Conference on Structural Stabilify and Dynamics, Taipei, Taiwan, pp. 703-708, 7-9 December 2000.

[20] Liu, G. R. and Gu, Y. T., "A matrix triangularization algorithm for point interpolation method, in Proc." Asia-Pacific Vibration Conference, Bangchun, W., Ed., November, Hangzhou, China, pp. 1151-1154, 2001.

[21] Liu, G. R. and Gu, Y. T., "A local radial point interpolation method (LR-PIM) for free vibration analyses of 2-D solids" Journal of Sound and Vibration, vol. 246, pp. 29-46, 2001.

[22] Liu, G. R. and Gu, Y. T., "Boundary meshfree methods based on the boundary point interpolation methods, Engineering Analysis with Boundary Elements, vol. 28, pp. 475-487, 2004.

[23] Liu, G. R. and Gu, Y.T., "A meshfree method: Meshfree Weak-Strong (MWS) form method, for 2-D solids", Computational Mechanics, vol. 33, pp. 2-14, 2003.

[24] Wang, J. G. and Liu, G. R., "A point interpolation meshless method based on radial basis functions", International Journal for Numerical Methods in Engineering, vol. 54, pp. 1623-1648, 2002.

[25] Kansa, E. J., "Multiquadrics - A Scattered Data Approximation Scheme with Applications to Computational Fluid-Dynamics - I," Computers & Mathematics with Applications, vol. 19, no. 8/9, pp. 127–145, 1990.

[26] Liu, G. R., "Mesh Free Methods - Moving beyond the Finite Element Method", First Edition, CRC Press, USA, 2003.

[27] T. Zhu, J. D. Zhang, and S. N. Atluri, "A local boundary integral equation (LBIE) method in computational mechanics and meshless discretization approach," Comput. Mech., vol. 21, pp. 223–235, 1998.

[28] Han, Z. D. and Atluri, S. N. “Meshless Local Petrov-Galerkin (MLPG) approaches for solving 3D Problems in elasto-statics”, Computer Modeling in Engineering and Science, vol.6, pp.169-188, 2004.

[30] Timoshenko, S. and Goodier, J., “Theory of Elasticity”, Third Edition, McGraw-Hill, New York, 1987.

[31] Wang, J.G. and Liu, G. R., “On the optimal shape parameters of radial basis functions used for 2-D meshless methods”, Comput. Methods Appl. Mech. Engrg., pp. 2611-2630, 2002.

[32] Liu, G. R. and Gu, Y. T., “An Introduction to Meshfree Methods and Their Programming”, First Edition, Springer, Netherlands, 2005.

[33] Li, S. and Liu, W. K., “Meshfree and Particle Methods and Their Applications”, App. Mech. Rev., vol.55, 2002.

[34] Liu, H. and Shi, P., “Meshfree Particle Method”, Proceedings of the Ninth IEEE International Conference on Computer Vision, vol.2, pp.289-296, 2003.

[35] Huerta, A., Belytschko, T., Fernandez-Mendez, S. and Rabczuk, T., “Meshfree Methods”, Encyclopedia of Computational Mechanics, 2004.